

Kirchhoff-Love shell theory based on tangential differential calculus

D. Schöllhammer, T.P. Fries

October 8, 2021

Institute of Structural Analysis
Graz University of Technology
Lessingstr. 25/II, 8010 Graz, Austria
www.ifb.tugraz.at
schoellhammer@tugraz.at

Abstract

The Kirchhoff-Love shell theory is recasted in the frame of the tangential differential calculus where differential operators on surfaces are formulated without the need for a parametrization, i.e., local coordinates. The governing equations are presented in strong and weak form including a detailed discussion of the boundary conditions and mechanical quantities such as moments, normal and shear forces. Although the parameter-free formulation leads to identical results than the classical formulation, it is more general as it applies also to shells whose geometry is implied by level-sets and, hence, no parametrization is available. Furthermore, it enables a different and unified view point on shell mechanics in general and leads to an elegant implementation. Numerical results are achieved based on isogeometric analysis for classical and new benchmark tests. Higher-order convergence rates in the residual errors are achieved when the physical fields are sufficiently smooth.

Keywords: Shells, Tangential Differential Calculus, Isogeometric analysis, Manifolds

Contents

1	Introduction	3
2	Preliminaries	5
2.1	Tangential Differential Calculus	6
3	The shell equations	12
3.1	Kinematics	12
3.2	Constitutive Equation	15
3.2.1	Stress resultants	15
3.3	Equilibrium	17
3.3.1	Equilibrium in weak form	17
3.3.2	Boundary conditions	18
4	Implementational aspects	21
5	Numerical results	23
5.1	Flat shell embedded in \mathbb{R}^3	24
5.2	Scordelis-Lo roof	28
5.3	Pinched cylinder	29
5.4	Flower shaped shell	30
6	Conclusions and Outlook	32
A	Element stiffness matrix	34
	References	37

1 Introduction

Classical shell mechanics relies on shell geometries resulting from a parametrization. That is, the middle surface is obtained by a map from some parameter space to the physical space, i.e., from mapping local (two-dimensional) to global (three-dimensional) coordinates, see Fig. 1(a). The introduction of co- and contra-variant base vectors is necessary and Christoffel symbols naturally occur. An overview in classical shell theory is given, e.g., in [41, 42, 9, 31, 4] or in the textbooks [1, 5, 38, 46].

It is important to note that a parametrization of the shell surface is not unique, hence, several parametrizations may describe the same geometry and, of course, must result in the same mechanical response of the shell. This is a clear hint that a parameter-independent shell formulation is possible. Even more so as shell geometries may also be implied by the level-set method [36, 40, 21, 22]; then, no parametrization exists but seeking the mechanical behaviour in this case is just as natural as in the parametrized case. For a long time, this distinction was may be less important, because it was found natural to generate a mesh for a shell geometry and perform a classical finite element analysis based on a surface mesh. Then, the mesh played the role of implying parametrizations anyway (from reference to physical elements), see Fig. 1(b), even if the shell geometry was initially defined by level-set functions. However, quite recently finite element approaches emerged which employ shape functions of (three-dimensional) background elements into which a curved surface is embedded, cf. Fig. 1(c). These functions are only evaluated on the surface where a surface model shall be solved and no parametrization (and surface mesh) is needed to furnish basis functions for the approximation. For these methods, e.g., labelled CutFEM [6, 8, 7] or TraceFEM [39, 23, 34, 35], applied to the case of shell mechanics, it is no longer necessary to rely on parameter-based formulations of the shell mechanics. A recent approach combines the idea of the CutFEM with isogeometric analysis [19].

This is not the first place where a parameter-free formulation of the Kirchhoff-Love shell theory is given, see, for instance, works by Delfour and Zolésio [11, 12, 13, 14]. This approach is also followed in [47, 32, 44] to model thin shells; membranes are considered in [25, 27]; curved beams are considered in [28]. A recent approach, which is limited to thin, flat shells embedded in \mathbb{R}^3 is given in [26]. However, previous approaches are often very technical and focus on mathematical properties rather than on the mechanical aspects. As such, the resulting formulations are often rather cumbersome and the simplicity and

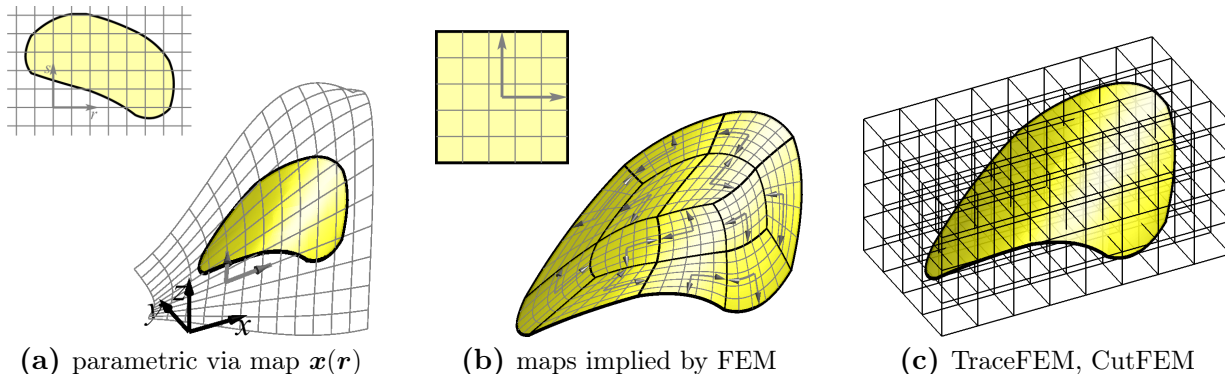


Fig. 1: (a) In classical shell mechanics, the middle surface is defined by a parametrization, i.e., a map $\mathbf{x}(\mathbf{r})$. (b) The surface mesh implies element-wise, approximate parametrizations even if the initial geometry is defined by level-sets. (c) For implicitly defined shells in the context of TraceFEM and CutFEM, no parametrization is needed at all.

elegance of the parameter-free formulation is less obvious. Herein, we consistently use the tangential differential calculus (TDC) based on surface differential operators such as surface gradients and divergence in combination with the tensor notation. The focus is on the mechanical modeling of the shell. For the first time, the parameter-free strong form of the Kirchhoff-Love shell is given and taken as the starting point to derive the weak form. Then, boundary terms for the relevant boundary conditions of Kirchhoff-Love shell theory are naturally achieved. Furthermore, mechanical quantities such as moments, normal and shear forces are defined based on global coordinates and it is shown how (parameter-)invariant quantities such as principal moments are computed. Finally, the strong form of Kirchhoff-Love shells is also found highly useful to define residual errors in the numerical results. Of course, evaluating this error in the strong form requires up to forth-order derivatives on the surface, which is implementationally quite some effort. The advantage, however, is that one may then confirm higher-order convergence rates in the corresponding error norm for suitable shell test cases. This is, otherwise, very difficult as exact solutions for shells are hardly available and classical benchmark tests typically give only selected scalar quantities, often with moderate accuracy.

The continuous weak form of the BVP is discretized with the surface FEM [18, 16, 20, 22] using NURBS as trial and test functions as proposed by Hughes et al. [29, 10] due to the continuity requirements of Kirchhoff-Love shells. The boundary conditions are weakly enforced via Lagrange multipliers [48]. The situation is very similar to [31], however, based on the proposed view point, the implementation is quite different. In particular, when PDEs on manifolds from other application fields than shell mechanics are also of interest

(e.g., when transport problems [17, 16, 18] or flow problems [20, 30] on curved surfaces are considered), there is a unified and elegant way to handle this by computing surface gradients applied to finite element shape functions which simplifies the situation considerably. In that sense one may shift significant parts of the implementation needed for shells to the underlying finite element technology and recycle this in other situations where PDEs on surfaces are considered.

The outline of the paper is as follows: In Section 2, important surface quantities are defined, and an introduction to the tangential differential calculus (TDC) is given. In Section 3, the classical linear Kirchhoff-Love shell equations under static loading are recast in terms of the TDC. Stress resultants such as membrane forces, bending moments, transverse shear forces and corner forces are defined. In Section 4, implementational aspects are considered. The element stiffness matrix and the resulting system of linear equations are shown. The implementation of boundary conditions based on Lagrange multipliers is outlined. Finally, in Section 5, numerical results are presented. The first example is a flat shell embedded in \mathbb{R}^3 , where an analytical solution is available. The second and third example are part of popular benchmarks as proposed in [2]. In the last example, a more general geometry without analytical solution or reference displacement is considered. The error is measured in the strong form of the equilibrium in order to verify the proposed approach and higher-order convergence rates are achieved.

2 Preliminaries

Shells are geometrical objects, where one dimension is significantly smaller compared to the other two dimensions. In this case, the shell can be reduced to a surface Γ embedded in the physical space \mathbb{R}^3 . In particular, the surface is a manifold of codimension 1. Let the surface be possibly curved, sufficiently smooth, orientable, connected and bounded by $\partial\Gamma$. There are two alternatives for defining the shell geometry. One is through a parametrization, i.e., a (bijective) mapping

$$\mathbf{x}(\boldsymbol{r}) : \hat{\Omega} \rightarrow \Gamma \tag{2.1}$$

from the parameter space $\hat{\Omega} \subset \mathbb{R}^2$ to the real domain $\Gamma \subset \mathbb{R}^3$. The other approach is based on the level-set method. Then, a level-set function $\phi(\mathbf{x})$ with $\mathbf{x} \in \Omega \subset \mathbb{R}^3$ exists and the

shell is implicitly given by

$$\Gamma = \{\mathbf{x} : \phi(\mathbf{x}) = 0 \quad \forall \mathbf{x} \in \Omega\} . \quad (2.2)$$

Additional level-set functions may restrict the zero-isosurface to the desired, bounded shell as described in [22]. In Fig. 2(a) and (b) the two different approaches are schematically shown.

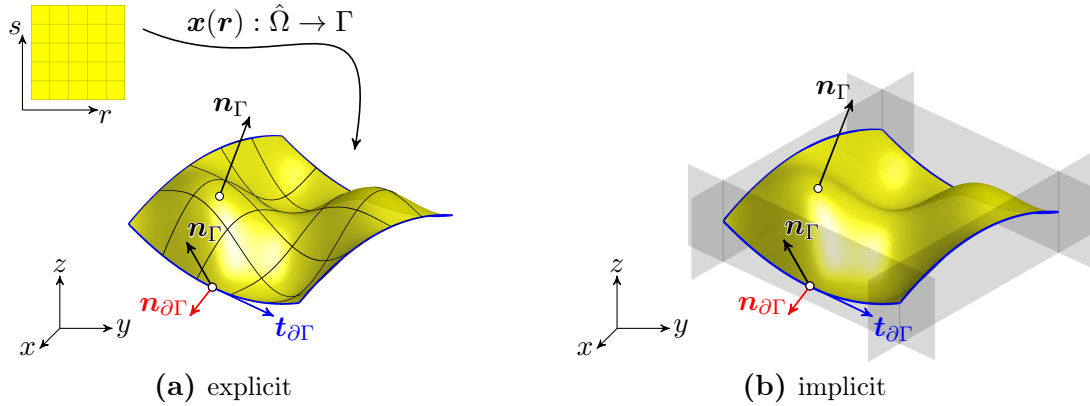


Fig. 2: Examples of bounded surfaces Γ embedded in the physical space \mathbb{R}^3 : (a) Explicitly defined surface with a map $\mathbf{x}(\mathbf{r})$, (b) Implicitly defined surface with a master level-function $\phi(\mathbf{x}) = 0$ (yellow) and slave level-set functions ψ_i for the boundary definition (gray).

In both cases, there exists a unit normal vector $\mathbf{n}_\Gamma = [n_x, n_y, n_z]^\top \in \mathbb{R}^3$. Along the boundary there is an associated tangential vector $\mathbf{t}_{\partial\Gamma} \in \mathbb{R}^3$ pointing in the direction of $\partial\Gamma$ and a co-normal vector $\mathbf{n}_{\partial\Gamma} = \mathbf{n}_\Gamma \times \mathbf{t}_{\partial\Gamma} \in \mathbb{R}^3$ pointing „outwards“ and being perpendicular to the boundary $\partial\Gamma$ yet in the tangent plane of the surface Γ . For the proof of equivalence of both cases we refer to, e.g., [18].

2.1 Tangential Differential Calculus

The TDC provides a framework to define differential operators avoiding the use of classical differential geometric methods based on local coordinate systems and Christoffel symbols. In the following, an overview of the operators and relations in the frame of the TDC are presented. For simplicity, we restrict ourselves to the case of surfaces embedded in the three dimensional space. However, the shown relations and definitions may be adopted to

other situations accordingly (e.g., curved lines embedded in 2D or 3D). An introduction from a more mathematical point of view is given in [15, 30].

Orthogonal projection operator \mathbf{P}

The orthogonal projection operator or normal projector $\mathbf{P} \in \mathbb{R}^{3 \times 3}$ is defined as

$$\mathbf{P} = \mathbb{I} - \mathbf{n}_\Gamma \otimes \mathbf{n}_\Gamma . \quad (2.3)$$

The operator \otimes is the dyadic product of two vectors. The normal projector \mathbf{P} projects a vector \mathbf{v} onto the tangent space $T_P\Gamma$ of the surface. Note that \mathbf{P} is idempotent ($\mathbf{P} \cdot \mathbf{P} = \mathbf{P}$), symmetric ($\mathbf{P} = \mathbf{P}^\top$) and obviously in the tangent space $T_P\Gamma$ of the surface, i.e., $\mathbf{P} \cdot \mathbf{n}_\Gamma = \mathbf{n}_\Gamma^\top \cdot \mathbf{P} = \mathbf{0}$.

The projection of a vector field $\mathbf{v} : \Gamma \rightarrow \mathbb{R}^3$ onto the tangent plane is defined by

$$\mathbf{v}_t = \mathbf{P} \cdot \mathbf{v} \in T_P\Gamma \quad (2.4)$$

where \mathbf{v}_t is tangential, i.e. $\mathbf{v}_t \cdot \mathbf{n}_\Gamma = 0$. The double projection of a second-order tensor function $\mathbf{A}(\mathbf{x}) : \Gamma \rightarrow \mathbb{R}^{3 \times 3}$ leads to an in-plane tensor and is defined as

$$\mathbf{A}_t = \mathbf{P} \cdot \mathbf{A} \cdot \mathbf{P} \in T_P\Gamma , \quad (2.5)$$

with the properties $\mathbf{A}_t = \mathbf{P} \cdot \mathbf{A}_t \cdot \mathbf{P}$ and $\mathbf{A}_t \cdot \mathbf{n}_\Gamma = \mathbf{n}_\Gamma^\top \cdot \mathbf{A}_t = \mathbf{0}$.

Tangential gradient of scalar functions

The tangential gradient ∇_Γ of a scalar function $u : \Gamma \rightarrow \mathbb{R}$ on the manifold is defined as

$$\nabla_\Gamma u(\mathbf{x}) = \mathbf{P}(\mathbf{x}) \cdot \nabla \tilde{u}(\mathbf{x}) , \quad \nabla_\Gamma u(\mathbf{x}) \in \mathbb{R}^{3 \times 1} , \quad \mathbf{x} \in \Gamma \quad (2.6)$$

where ∇ is the standard gradient operator in the physical space and \tilde{u} is a smooth extension of u in a neighbourhood \mathcal{U} of the manifold Γ . Alternatively, \tilde{u} is given as a function in global coordinates $\tilde{u}(\mathbf{x}) : \mathbb{R}^3 \rightarrow \mathbb{R}$ and only evaluated at the manifold $\tilde{u}|_\Gamma = u$.

For parametrized surfaces defined by the map $\mathbf{x}(\mathbf{r})$, and a given scalar function $u(\mathbf{r}) : \hat{\Omega} \rightarrow \mathbb{R}$, the tangential gradient can be determined without explicitly computing an extension \tilde{u}

using

$$\nabla_{\Gamma} u(\mathbf{x}(\mathbf{r})) = \mathbf{J}(\mathbf{r}) \cdot \mathbf{G}(\mathbf{r})^{-1} \cdot \nabla_{\mathbf{r}} u(\mathbf{r}) , \quad (2.7)$$

with $\mathbf{J}(\mathbf{r}) = \partial \mathbf{x} / \partial \mathbf{r} \in \mathbb{R}^{3 \times 2}$ being the Jacobi-matrix, $\mathbf{G} = \mathbf{J}^T \cdot \mathbf{J}$ is the metric tensor or the first fundamental form and the operator $\nabla_{\mathbf{r}}$ is the gradient with respect to the reference coordinates. The components of the tangential gradient are denoted by

$$\nabla_{\Gamma} u = \begin{bmatrix} \partial_x^{\Gamma} u \\ \partial_y^{\Gamma} u \\ \partial_z^{\Gamma} u \end{bmatrix} , \quad (2.8)$$

representing first-order partial tangential derivatives. An important property of $\nabla_{\Gamma} u$ is that the tangential gradient of a scalar valued function is in the tangent space of the surface $\nabla_{\Gamma} u \in T_P \Gamma$, i.e., $\nabla_{\Gamma} u \cdot \mathbf{n}_{\Gamma} = 0$. When using the FEM to solve BVPs on surfaces, one may use Eq. 2.7 to compute tangential gradients of the shape functions.

Tangential gradient of vector-valued functions

Consider a vector-valued function $\mathbf{v}(\mathbf{x}) : \Gamma \rightarrow \mathbb{R}^3$ and apply to each component of \mathbf{v} the tangential gradient for scalars. This leads to the *directional* gradient of \mathbf{v} defined as

$$\nabla_{\Gamma}^{\text{dir}} \mathbf{v}(\mathbf{x}) = \nabla_{\Gamma}^{\text{dir}} \begin{bmatrix} u(\mathbf{x}) \\ v(\mathbf{x}) \\ w(\mathbf{x}) \end{bmatrix} = \begin{bmatrix} \partial_x^{\Gamma} u & \partial_y^{\Gamma} u & \partial_z^{\Gamma} u \\ \partial_x^{\Gamma} v & \partial_y^{\Gamma} v & \partial_z^{\Gamma} v \\ \partial_x^{\Gamma} w & \partial_y^{\Gamma} w & \partial_z^{\Gamma} w \end{bmatrix} . \quad (2.9)$$

Note that the directional gradient is *not* in the tangent space of the surface, in general. A projection of the directional gradient to the tangent space leads to the *covariant* gradient of \mathbf{v} and is defined as

$$\nabla_{\Gamma}^{\text{cov}} \mathbf{v} = \mathbf{P} \cdot \nabla_{\Gamma}^{\text{dir}} \mathbf{v} , \quad (2.10)$$

which is an in-plane tensor, i.e., $\nabla_{\Gamma}^{\text{cov}} \mathbf{v} \in T_P \Gamma$. The covariant gradient often appears in the modelling of physical phenomena on manifolds, i.e., in the governing equations. In contrast the directional gradient appears naturally in product rules or divergence theorems on manifolds.

In the following, partial surface derivatives of scalar functions are denoted as $\partial_{x_i}^\Gamma u$ or $u_{,i}^\Gamma$ with $i = 1, 2, 3$. Partial surface derivatives of vector or tensor components are denoted as $v_{i,j}^{\text{dir}}$ for directional and $v_{i,j}^{\text{cov}}$ for covariant derivatives with $i, j = 1, 2, 3$.

Tangential gradient of tensor functions

For a second-order tensor function $\mathbf{A}(\mathbf{x}) : \Gamma \rightarrow \mathbb{R}^{3 \times 3}$, the partial directional gradient with respect to x_i is defined as

$$\nabla_{\Gamma,i}^{\text{dir}} \mathbf{A} = \frac{\partial \mathbf{A}}{\partial x_i} = \begin{bmatrix} \partial_{x_i}^\Gamma A_{11} & \partial_{x_i}^\Gamma A_{12} & \partial_{x_i}^\Gamma A_{13} \\ \partial_{x_i}^\Gamma A_{21} & \partial_{x_i}^\Gamma A_{22} & \partial_{x_i}^\Gamma A_{23} \\ \partial_{x_i}^\Gamma A_{31} & \partial_{x_i}^\Gamma A_{32} & \partial_{x_i}^\Gamma A_{33} \end{bmatrix} \quad \text{with: } i = 1, 2, 3. \quad (2.11)$$

The directional gradient of the tensor function is then defined as

$$\nabla_\Gamma^{\text{dir}} \mathbf{A} = (\nabla_{\Gamma,1}^{\text{dir}} \mathbf{A} \quad \nabla_{\Gamma,2}^{\text{dir}} \mathbf{A} \quad \nabla_{\Gamma,3}^{\text{dir}} \mathbf{A}) . \quad (2.12)$$

The covariant partial derivative is determined by projecting the partial directional derivative onto the tangent space

$$\nabla_{\Gamma,i}^{\text{cov}} \mathbf{A} = \mathbf{P} \cdot \nabla_{\Gamma,i}^{\text{dir}} \mathbf{A} \cdot \mathbf{P} . \quad (2.13)$$

Second-order tangential derivatives

Next, second-order derivatives of scalar functions are considered. The directional second order gradient of a scalar function u is defined by

$$\{\mathbf{He}^{\text{dir}}\}_{ij}(u(\mathbf{x})) = \partial_{x_j}^{\Gamma, \text{dir}} (\partial_{x_i}^\Gamma u(\mathbf{x})) = u_{,ji}^{\text{dir}} = \begin{bmatrix} \partial_{xx}^\Gamma u & \partial_{yx}^\Gamma u & \partial_{zx}^\Gamma u \\ \partial_{xy}^\Gamma u & \partial_{yy}^\Gamma u & \partial_{zy}^\Gamma u \\ \partial_{xz}^\Gamma u & \partial_{yz}^\Gamma u & \partial_{zz}^\Gamma u \end{bmatrix} = \nabla_\Gamma^{\text{dir}} (\nabla_\Gamma u(\mathbf{x})) \quad (2.14)$$

where \mathbf{He}^{dir} is the tangential Hessian matrix which is not symmetric in the case of curved manifolds [15], i.e., $u_{,ij}^{\text{dir}} \neq u_{,ji}^{\text{dir}}$. For the case of parametrized surfaces and a given scalar

function in the reference space, the tangential Hessian-matrix can be determined by

$$\begin{aligned} \mathbf{He}^{\text{dir}}(u) &= \nabla_{\Gamma}^{\text{dir}} (\mathbf{Q} \cdot \nabla_r u) \\ &= [\mathbf{Q}_{,r} \cdot \nabla_r u \quad \mathbf{Q}_{,s} \cdot \nabla_r u] \cdot \mathbf{Q}^{\top} + \mathbf{Q} \cdot \nabla_r (\nabla_r u) \cdot \mathbf{Q}^{\top} \end{aligned} \quad (2.15)$$

where, $\mathbf{Q} = \mathbf{J} \cdot \mathbf{G}^{-1}$, and $\mathbf{Q}_{,r_i}$ denotes the partial tangential derivative of \mathbf{Q} with respect to r_i . The covariant counterpart is

$$\mathbf{He}^{\text{cov}}(u) = \nabla_{\Gamma}^{\text{cov}} (\nabla_{\Gamma} u) = \mathbf{P} \cdot \nabla_{\Gamma}^{\text{dir}} (\nabla_{\Gamma} u) = \mathbf{P} \cdot \mathbf{He}^{\text{dir}}(u) . \quad (2.16)$$

In contrast to \mathbf{He}^{dir} , \mathbf{He}^{cov} is symmetric and an in-plane tensor [45]. In the special case of flat surfaces embedded in \mathbb{R}^3 the directional and covariant Hessian matrix are equal.

Tangential divergence operators

The divergence operator of a vector valued function $\mathbf{v}(\mathbf{x}) : \Gamma \rightarrow \mathbb{R}^3$ is given as

$$\text{div}_{\Gamma} \mathbf{v}(\mathbf{x}) = \text{tr} (\nabla_{\Gamma}^{\text{dir}} \mathbf{v}(\mathbf{x})) = \text{tr} (\nabla_{\Gamma}^{\text{cov}} \mathbf{v}(\mathbf{x})) , \quad (2.17)$$

and the divergence of a matrix or tensor function $\mathbf{A}(\mathbf{x}) : \Gamma \rightarrow \mathbb{R}^{3 \times 3}$, is

$$\text{div}_{\Gamma} \mathbf{A}(\mathbf{x}) = \begin{bmatrix} \text{div}_{\Gamma} [A_{11}, A_{12}, A_{13}] \\ \text{div}_{\Gamma} [A_{21}, A_{22}, A_{23}] \\ \text{div}_{\Gamma} [A_{31}, A_{32}, A_{33}] \end{bmatrix} . \quad (2.18)$$

Note that $\text{div}_{\Gamma} \mathbf{A}$ is, in general, not a tangential vector. It would only be tangential if the surface is flat and \mathbf{A} is an in-plane tensor.

Weingarten map and curvature

The Weingarten map as introduced in [30, 15] is defined as

$$\mathbf{H} = \nabla_{\Gamma}^{\text{dir}} \mathbf{n}_{\Gamma} = \nabla_{\Gamma}^{\text{cov}} \mathbf{n}_{\Gamma} \quad (2.19)$$

and is related to the second fundamental form in differential geometry. The Weingarten map is a symmetric, in-plane tensor and its two non-zero eigenvalues are associated with

the principles curvatures

$$\kappa_{1,2} = -\text{eig}(\mathbf{H}) . \quad (2.20)$$

The minus in Eq. 2.20 is due to fact that the Weingarten map is defined with the „outward“ unit normal vector instead of the „inward“ unit normal vector, which leads to positive curvatures of a sphere. The third eigenvalue is zero, because \mathbf{H} is an in-plane tensor. The corresponding eigenvectors \mathbf{t}_1 , \mathbf{t}_2 and \mathbf{n}_Γ are perpendicular as \mathbf{H} is symmetric. In Fig. 3, the osculating circles with the radii $r_i = 1/\kappa_i$ and the eigenvectors at a point \mathbf{P} are shown.

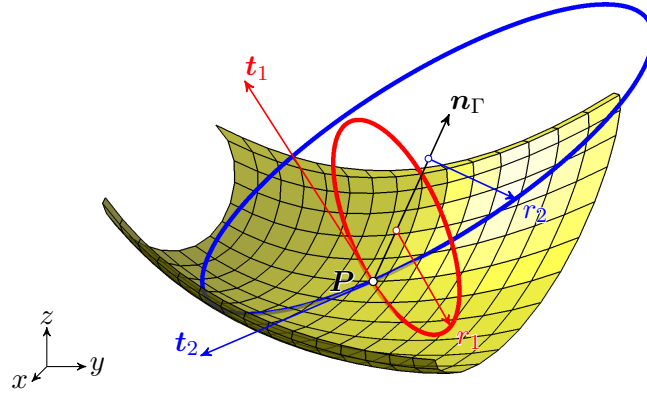


Fig. 3: Osculating circles (blue, red) and eigenvectors (\mathbf{t}_1 , \mathbf{t}_2 , \mathbf{n}_Γ) of \mathbf{H} at point \mathbf{P} on a surface embedded in \mathbb{R}^3 .

The Gauß curvature is defined as the product of the principle curvatures $K = \prod_{i=1}^2 \kappa_i$ and the mean curvature is introduced as $\varkappa = \kappa_1 + \kappa_2 = \text{tr}(\mathbf{H})$.

Divergence theorems in terms of tangential operators

The divergence theorem or Green's formula for a scalar function $f \in C^1(\Gamma)$ and a vector valued function $\mathbf{v} \in C^1(\Gamma)^3$ are defined as in [13, 15]

$$\int_{\Gamma} f \cdot \text{div}_{\Gamma} \mathbf{v} \, d\Gamma = - \int_{\Gamma} \nabla_{\Gamma} f \cdot \mathbf{v} \, d\Gamma + \int_{\Gamma} \varkappa f (\mathbf{v} \cdot \mathbf{n}_{\Gamma}) \, d\Gamma + \int_{\partial\Gamma} f \mathbf{v} \cdot \mathbf{n}_{\partial\Gamma} \, d\partial\Gamma . \quad (2.21)$$

The term with the mean curvature \varkappa is vanishing if the vector \mathbf{v} is tangential, then $\mathbf{v} \cdot \mathbf{n}_{\Gamma} = 0$. In extension to Eq. 2.21, Green's formula for second order tensor functions

$\mathbf{A} \in C^1(\Gamma)^{3 \times 3}$, is

$$\int_{\Gamma} \mathbf{v} \cdot \operatorname{div}_{\Gamma} \mathbf{A} \, d\Gamma = - \int_{\Gamma} \nabla_{\Gamma}^{\operatorname{dir}} \mathbf{v} : \mathbf{A} \, d\Gamma + \int_{\Gamma} \varkappa \mathbf{v} \cdot (\mathbf{A} \cdot \mathbf{n}_{\Gamma}) \, d\Gamma + \int_{\partial\Gamma} \mathbf{v} \cdot (\mathbf{A} \cdot \mathbf{n}_{\partial\Gamma}) \, d\partial\Gamma \quad (2.22)$$

where $\nabla_{\Gamma}^{\operatorname{dir}} \mathbf{v} : \mathbf{A} = \operatorname{tr}(\nabla_{\Gamma}^{\operatorname{dir}} \mathbf{v} \cdot \mathbf{A}^{\top})$. In the case of in-plane tensors, e.g., $\mathbf{A}_t = \mathbf{P} \cdot \mathbf{A}_t \cdot \mathbf{P}$, the term with the mean curvature \varkappa vanishes due to $\mathbf{A}_t \cdot \mathbf{n}_{\Gamma} = \mathbf{0}$ and we also have $\nabla_{\Gamma}^{\operatorname{dir}} \mathbf{v} : \mathbf{A}_t = \nabla_{\Gamma}^{\operatorname{cov}} \mathbf{v} : \mathbf{A}_t$.

3 The shell equations

In this section, we derive the linear Kirchhoff-Love shell theory in the frame of tangential operators based on a global Cartesian coordinate system. We restrict ourselves to infinitesimal deformations, which means that the reference and spatial configuration are indistinguishable. Furthermore, a linear elastic material governed by Hooke's law is assumed. As usual in the Kirchhoff-Love shell theory, the transverse shear strains and the change of curvature in the material law may be neglected, which restricts the model to thin shells ($t\kappa_{\max} \ll 1$).

With these assumptions, an analytical pre-integration with respect to the thickness leads to stress resultants such as normal forces and bending moments. The equilibrium in strong form is then expressed in terms of the stress resultants. Finally, the transverse shear forces may be identified via equilibrium considerations.

3.1 Kinematics

The middle surface Γ of the shell is a sufficiently smooth manifold embedded in the physical space \mathbb{R}^3 . A point on the middle surface is denoted as $\mathbf{x}_{\Gamma} \in \Gamma \subset \mathbb{R}^3$ and may be obtained explicitly or implicitly, see Section 2. With the unit-normal vector \mathbf{n}_{Γ} a point in the domain of the shell Ω of thickness t is defined by

$$\mathbf{x} = \mathbf{x}_{\Gamma} + \zeta \mathbf{n}_{\Gamma} \quad (3.1)$$

with ζ being the thickness parameter and $|\zeta| \leq t/2$. Alternatively, if the middle surface is defined implicitly with a signed distance function $\phi(\mathbf{x})$ the domain of the shell Ω is defined by

$$\Omega = \left\{ \mathbf{x} \in \mathbb{R}^3 : |\phi(\mathbf{x})| \leq \frac{t}{2} \right\}. \quad (3.2)$$

In this case the middle surface Γ is the zero-isosurface of $\phi(\mathbf{x})$, see Eq. 2.2. The displacement field \mathbf{u}_Ω of a point $\mathbf{P}(\mathbf{x}_\Gamma, \zeta)$ in the shell continuum Ω takes the form

$$\mathbf{u}_\Omega(\mathbf{x}_\Gamma, \zeta) = \mathbf{u}(\mathbf{x}_\Gamma) + \zeta \mathbf{w}(\mathbf{x}_\Gamma) \quad (3.3)$$

with $\mathbf{u}(\mathbf{x}_\Gamma) = [u, v, w]^\top$ being the displacement field of the middle surface and $\mathbf{w}(\mathbf{x}_\Gamma)$ being the difference vector, as illustrated in Fig. 4.

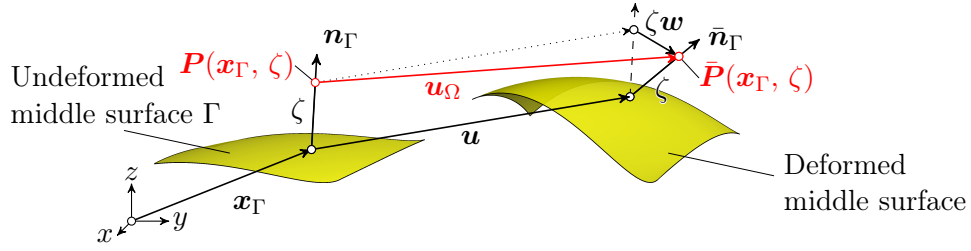


Fig. 4: Displacements \mathbf{u}_Ω , \mathbf{u} and \mathbf{w} of the shell.

Without transverse shear strains, the difference vector \mathbf{w} expressed in terms of TDC is defined as in [13]

$$\mathbf{w}(\mathbf{x}_\Gamma) = - \left[\nabla_\Gamma^{\text{dir}} \mathbf{u} + (\nabla_\Gamma^{\text{dir}} \mathbf{u})^\top \right] \cdot \mathbf{n}_\Gamma = \mathbf{H} \cdot \mathbf{u} - \nabla_\Gamma(\mathbf{u} \cdot \mathbf{n}_\Gamma). \quad (3.4)$$

As readily seen in the equation above, the difference vector \mathbf{w} is tangential. Alternatively, the difference vector \mathbf{w} may also be re-written in terms of partial tangential derivatives of \mathbf{u} and the normal vector \mathbf{n}_Γ

$$\mathbf{w}(\mathbf{x}_\Gamma) = \mathbf{H} \cdot \mathbf{u} - \nabla_\Gamma(\mathbf{u} \cdot \mathbf{n}_\Gamma) = - \begin{bmatrix} \mathbf{u}_{,x}^{\text{dir}} \cdot \mathbf{n}_\Gamma \\ \mathbf{u}_{,y}^{\text{dir}} \cdot \mathbf{n}_\Gamma \\ \mathbf{u}_{,z}^{\text{dir}} \cdot \mathbf{n}_\Gamma \end{bmatrix}. \quad (3.5)$$

Consequently, the displacement field of the shell continuum is only a function of the middle surface displacement \mathbf{u} , the unit normal vector \mathbf{n}_Γ and the thickness parameter ζ .

The linearised, in-plane strain tensor $\boldsymbol{\varepsilon}_\Gamma$ is defined by the symmetric part of the directional gradient of the displacement field \mathbf{u}_Ω , projected with \mathbf{P} [25]

$$\begin{aligned}\boldsymbol{\varepsilon}_\Gamma(\mathbf{x}_\Gamma, \zeta) &= \mathbf{P} \cdot \frac{1}{2} [\nabla_\Gamma^{\text{dir}} \mathbf{u}_\Omega + (\nabla_\Gamma^{\text{dir}} \mathbf{u}_\Omega)^\top] \cdot \mathbf{P} = \mathbf{P} \cdot \boldsymbol{\varepsilon}_\Gamma^{\text{dir}} \cdot \mathbf{P} \\ &= \frac{1}{2} [\nabla_\Gamma^{\text{cov}} \mathbf{u}_\Omega + (\nabla_\Gamma^{\text{cov}} \mathbf{u}_\Omega)^\top] .\end{aligned}\tag{3.6}$$

Finally, the whole strain tensor may be split into a membrane and bending part, as usual in the classical theory

$$\boldsymbol{\varepsilon}_\Gamma = \boldsymbol{\varepsilon}_{\Gamma, \text{M}}(\mathbf{u}) + \zeta \boldsymbol{\varepsilon}_{\Gamma, \text{B}}(\mathbf{w}) ,\tag{3.7}$$

with

$$\begin{aligned}\boldsymbol{\varepsilon}_{\Gamma, \text{M}} &= \frac{1}{2} (\nabla_\Gamma^{\text{cov}} \mathbf{u} + (\nabla_\Gamma^{\text{cov}} \mathbf{u})^\top) , \\ \boldsymbol{\varepsilon}_{\Gamma, \text{B}} &= - \begin{bmatrix} \mathbf{u}_{,xx}^{\text{cov}} \cdot \mathbf{n}_\Gamma & \mathbf{u}_{,yx}^{\text{cov}} \cdot \mathbf{n}_\Gamma & \mathbf{u}_{,zx}^{\text{cov}} \cdot \mathbf{n}_\Gamma \\ & \mathbf{u}_{,yy}^{\text{cov}} \cdot \mathbf{n}_\Gamma & \mathbf{u}_{,zy}^{\text{cov}} \cdot \mathbf{n}_\Gamma \\ \text{sym} & & \mathbf{u}_{,zz}^{\text{cov}} \cdot \mathbf{n}_\Gamma \end{bmatrix} .\end{aligned}$$

Note that in the linearised bending strain tensor $\boldsymbol{\varepsilon}_{\Gamma, \text{B}}$, the term $(\nabla_\Gamma^{\text{dir}} \mathbf{u})^\top \cdot \mathbf{H}$ is neglected as in classical theory [42, Remark 2.2] or [46]. The resulting membrane and bending strain in Eq. 3.7 are equivalent compared to the classical theory, e.g., [1]. In the case of flat shell structures as considered in [26] the membrane strain is only a function of the tangential displacement $\mathbf{u}_t = \mathbf{P} \cdot \mathbf{u}$ and the bending strain only depends on the normal displacement $u_n = \mathbf{u} \cdot \mathbf{n}_\Gamma$, which simplifies the whole kinematic significantly. Moreover, the normal vector \mathbf{n}_Γ is then constant and the difference vector simplifies to $\mathbf{w}(\mathbf{x}_\Gamma) = -\nabla_\Gamma u_n$.

3.2 Constitutive Equation

As already mentioned above, the shell is assumed to be linear elastic and, as usual for thin structures, plane stress is presumed. The in-plane stress tensor $\boldsymbol{\sigma}_\Gamma$ is defined as

$$\boldsymbol{\sigma}_\Gamma(\mathbf{x}_\Gamma, \zeta) = \mathbf{P} \cdot [2\mu\boldsymbol{\varepsilon}_\Gamma + \lambda\text{tr}(\boldsymbol{\varepsilon}_\Gamma)\mathbb{I}] \cdot \mathbf{P} \quad (3.8)$$

$$= \mathbf{P} \cdot [2\mu\boldsymbol{\varepsilon}_\Gamma^{\text{dir}} + \lambda\text{tr}(\boldsymbol{\varepsilon}_\Gamma^{\text{dir}})\mathbb{I}] \cdot \mathbf{P} \quad (3.9)$$

where $\mu = \frac{E}{2(1+\nu)}$ and $\lambda = \frac{E\nu}{(1-\nu^2)}$ are the Lamé constants and $\boldsymbol{\varepsilon}_\Gamma^{\text{dir}}$ is the directional strain tensor from Eq. 3.6. With this identity the in-plane stress tensor can be computed only with the directional strain tensor

$$\boldsymbol{\varepsilon}_\Gamma^{\text{dir}} = \boldsymbol{\varepsilon}_{\Gamma,\text{M}}^{\text{dir}}(\mathbf{u}) + \zeta\boldsymbol{\varepsilon}_{\Gamma,\text{B}}^{\text{dir}}(\mathbf{w}) ,$$

with

$$\boldsymbol{\varepsilon}_{\Gamma,\text{M}}^{\text{dir}} = \frac{1}{2}(\nabla_\Gamma^{\text{dir}}\mathbf{u} + (\nabla_\Gamma^{\text{dir}}\mathbf{u})^\top) ,$$

$$\boldsymbol{\varepsilon}_{\Gamma,\text{B}}^{\text{dir}} = - \begin{bmatrix} \mathbf{u}_{,xx}^{\text{dir}} \cdot \mathbf{n}_\Gamma & \frac{1}{2}(\mathbf{u}_{,yx}^{\text{dir}} + \mathbf{u}_{,xy}^{\text{dir}}) \cdot \mathbf{n}_\Gamma & \frac{1}{2}(\mathbf{u}_{,zx}^{\text{dir}} + \mathbf{u}_{,xz}^{\text{dir}}) \cdot \mathbf{n}_\Gamma \\ & \mathbf{u}_{,yy}^{\text{dir}} \cdot \mathbf{n}_\Gamma & \frac{1}{2}(\mathbf{u}_{,zy}^{\text{dir}} + \mathbf{u}_{,yz}^{\text{dir}}) \cdot \mathbf{n}_\Gamma \\ \text{sym} & & \mathbf{u}_{,zz}^{\text{dir}} \cdot \mathbf{n}_\Gamma \end{bmatrix} ,$$

which is from an implementational point of view an advantage, because covariant derivatives are not needed explicitly. In comparison to the classical theory, the in-plane stress tensor expressed in terms of TDC does not require the computation of the metric coefficients in the material law. Therefore, the resulting stress tensor does not hinge on a parametrization of the middle surface and shell analysis on implicitly defined surfaces is enabled.

3.2.1 Stress resultants

The stress tensor is only a function of the middle surface displacement vector \mathbf{u} , the difference vector $\mathbf{w}(\mathbf{u})$ and the thickness parameter ζ . This enables an analytical pre-integration with respect to the thickness and stress resultants can be identified. The following quantities are equivalent to the stress resultants in the classical theory [42, 1], but they are expressed in terms of the TDC using a global Cartesian coordinate system.

The moment tensor \mathbf{m}_Γ is defined as

$$\mathbf{m}_\Gamma = \int_{-t/2}^{t/2} \zeta \boldsymbol{\sigma}_\Gamma(\mathbf{u}, \zeta) \, d\zeta = \frac{t^3}{12} \boldsymbol{\sigma}_\Gamma(\boldsymbol{\varepsilon}_{\Gamma,B}) = \mathbf{P} \cdot \mathbf{m}_\Gamma^{\text{dir}} \cdot \mathbf{P} , \quad (3.10)$$

with

$$\mathbf{m}_\Gamma^{\text{dir}} = -D \begin{bmatrix} (\mathbf{u}_{,xx}^{\text{dir}} + \nu \mathbf{u}_{,yy}^{\text{dir}} + \nu \mathbf{u}_{,zz}^{\text{dir}}) \cdot \mathbf{n}_\Gamma & \frac{1-\nu}{2} (\mathbf{u}_{,yx}^{\text{dir}} + \mathbf{u}_{,xy}^{\text{dir}}) \cdot \mathbf{n}_\Gamma & \frac{1-\nu}{2} (\mathbf{u}_{,zx}^{\text{dir}} + \mathbf{u}_{,xz}^{\text{dir}}) \cdot \mathbf{n}_\Gamma \\ & (\mathbf{u}_{,yy}^{\text{dir}} + \nu \mathbf{u}_{,xx}^{\text{dir}} + \nu \mathbf{u}_{,zz}^{\text{dir}}) \cdot \mathbf{n}_\Gamma & \frac{1-\nu}{2} (\mathbf{u}_{,zy}^{\text{dir}} + \mathbf{u}_{,yz}^{\text{dir}}) \cdot \mathbf{n}_\Gamma \\ & \text{sym.} & (\mathbf{u}_{,zz}^{\text{dir}} + \nu \mathbf{u}_{,xx}^{\text{dir}} + \nu \mathbf{u}_{,yy}^{\text{dir}}) \cdot \mathbf{n}_\Gamma \end{bmatrix}$$

where $D = \frac{Et^3}{12(1-\nu^2)}$ is the flexural rigidity of the shell. The moment tensor \mathbf{m}_Γ is symmetric and an in-plane tensor. Therefore, one of the three eigenvalues is zero and the two non-zero eigenvalues of \mathbf{m}_Γ are the principle bending moments m_1 and m_2 . The principle moments are in agreement with the eigenvalues of the moment tensor in the classical setting, see [1]. For the effective normal force tensor $\tilde{\mathbf{n}}_\Gamma$ we have

$$\tilde{\mathbf{n}}_\Gamma = \int_{-t/2}^{t/2} \boldsymbol{\sigma}_\Gamma(\mathbf{u}, \zeta) \, d\zeta = t \boldsymbol{\sigma}_\Gamma(\boldsymbol{\varepsilon}_{\Gamma,M}) = \mathbf{P} \cdot \mathbf{n}_\Gamma^{\text{dir}} \cdot \mathbf{P} , \quad (3.11)$$

with

$$\mathbf{n}_\Gamma^{\text{dir}} = \frac{Et}{1-\nu^2} \begin{bmatrix} u_{,x}^{\text{dir}} + \nu(v_{,y}^{\text{dir}} + w_{,z}^{\text{dir}}) & \frac{1-\nu}{2}(u_{,y}^{\text{dir}} + v_{,x}^{\text{dir}}) & \frac{1-\nu}{2}(u_{,z}^{\text{dir}} + w_{,x}^{\text{dir}}) \\ & v_{,y}^{\text{dir}} + \nu(u_{,x}^{\text{dir}} + w_{,z}^{\text{dir}}) & \frac{1-\nu}{2}(v_{,z}^{\text{dir}} + w_{,y}^{\text{dir}}) \\ & \text{sym} & w_{,z}^{\text{dir}} + \nu(u_{,x}^{\text{dir}} + v_{,y}^{\text{dir}}) \end{bmatrix} .$$

Similar to the moment tensor, the two non-zero eigenvalues of $\tilde{\mathbf{n}}_\Gamma$ are in agreement with the effective normal force tensor expressed in local coordinates. Note that for curved shells this tensor is *not* the physical normal force tensor. This tensor only appears in the variational formulation, see Section 4. The physical normal force tensor $\mathbf{n}_\Gamma^{\text{real}}$ is defined by

$$\mathbf{n}_\Gamma^{\text{real}} = \tilde{\mathbf{n}}_\Gamma + \mathbf{H} \cdot \mathbf{m}_\Gamma \quad (3.12)$$

and is, in general, not symmetric and also has one zero eigenvalue. The occurrence of the zero eigenvalues in \mathbf{m}_Γ , $\tilde{\mathbf{n}}_\Gamma$ and $\mathbf{n}_\Gamma^{\text{real}}$ is due to fact that these tensors are in-plane tensors, i.e. $\mathbf{m}_\Gamma \cdot \mathbf{n}_\Gamma = \mathbf{n}_\Gamma^\top \cdot \mathbf{m}_\Gamma = \mathbf{0}$. The normal vector \mathbf{n}_Γ is the corresponding eigenvector to the

zero eigenvalue and the other two eigenvectors are tangential.

3.3 Equilibrium

Based on the stress resultants from above, one obtains the equilibrium for a curved shell in strong form as

$$\operatorname{div}_\Gamma \tilde{\mathbf{n}}_\Gamma + \mathbf{n}_\Gamma \operatorname{div}_\Gamma (\mathbf{P} \cdot \operatorname{div}_\Gamma \mathbf{m}_\Gamma) + 2\mathbf{H} \cdot \operatorname{div}_\Gamma \mathbf{m}_\Gamma + [\partial x_i^\Gamma \mathbf{H}]_{jk} [\mathbf{m}_\Gamma]_{ki} = -\mathbf{f} , \quad (3.13)$$

with \mathbf{f} being the load vector per area on the middle surface Γ . A summation over the indices $i, k = 1, 2, 3$ has to be performed. The obtained equilibrium does not rely on a parametrization of the middle surface but is, otherwise, equivalent to the equilibrium in local coordinates [1, 46]. From this point of view, the reformulation of the linear Kirchhoff-Love shell equations in terms of the TDC may be seen as a generalization, because the requirement of a parametrized middle surface is circumvented. With boundary conditions, as shown in detail in Section 3.3.2, the complete fourth-order boundary value problem (BVP) is defined.

Based on the equilibrium in Eq. 3.13, the transverse shear force vector \mathbf{q} is defined as

$$\mathbf{q} = \mathbf{P} \cdot \operatorname{div}_\Gamma \mathbf{m}_\Gamma . \quad (3.14)$$

Note that in the special case of *flat* Kirchhoff-Love structures embedded in \mathbb{R}^3 the divergence of an in-plane tensor is a tangential vector, as already mentioned in Section 2.1. Therefore, the definition of the transverse shear force vector in [26] is in agreement with the obtained transverse shear force vector herein.

3.3.1 Equilibrium in weak form

The equilibrium in strong form is converted to a weak form by multiplying Eq. 3.13 with a suitable test function \mathbf{v} and integrating over the domain, leading to

$$\begin{aligned} - \int_\Gamma \mathbf{v} \cdot \{ \operatorname{div}_\Gamma \tilde{\mathbf{n}}_\Gamma + \mathbf{n}_\Gamma \operatorname{div}_\Gamma (\mathbf{P} \cdot \operatorname{div}_\Gamma \mathbf{m}_\Gamma) + 2\mathbf{H} \cdot \operatorname{div}_\Gamma \mathbf{m}_\Gamma + [\partial x_i^\Gamma \mathbf{H}]_{jk} [\mathbf{m}_\Gamma]_{ki} \} \, d\Gamma = \\ = \int_\Gamma \mathbf{v} \cdot \mathbf{f} \, d\Gamma . \end{aligned} \quad (3.15)$$

With Green's formula from Section 2.1, we introduce the continuous weak form of the equilibrium:

Find $\mathbf{u} \in \mathcal{V} : \Gamma \rightarrow \mathbb{R}^3$ such that

$$a(\mathbf{u}, \mathbf{v}) = \langle \mathbf{F}, \mathbf{v} \rangle \quad \forall \mathbf{v} \in \mathcal{V}_0, \quad (3.16)$$

with

$$\begin{aligned} a(\mathbf{u}, \mathbf{v}) &= \int_{\Gamma} \nabla_{\Gamma}^{\text{dir}} \mathbf{v} : \tilde{\mathbf{n}}_{\Gamma} - \boldsymbol{\varepsilon}_{\Gamma, \text{B}}^{\text{dir}}(\mathbf{v}) : \mathbf{m}_{\Gamma} \, d\Gamma, \\ \langle \mathbf{F}, \mathbf{v} \rangle &= \int_{\Gamma} \mathbf{f} \cdot \mathbf{v} \, d\Gamma + \int_{\partial\Gamma_{\text{N}}} \nabla_{\Gamma}^{\text{dir}}(\mathbf{v} \cdot \mathbf{n}_{\Gamma}) \cdot (\mathbf{m}_{\Gamma} \cdot \mathbf{n}_{\partial\Gamma}) - 2(\mathbf{H} \cdot \mathbf{v}) \cdot (\mathbf{m}_{\Gamma} \cdot \mathbf{n}_{\partial\Gamma}) - \\ &\quad \mathbf{v} \cdot (\tilde{\mathbf{n}}_{\Gamma} \cdot \mathbf{n}_{\partial\Gamma}) - (\mathbf{v} \cdot \mathbf{n}_{\Gamma}) (\mathbf{P} \cdot \text{div}_{\Gamma} \mathbf{m}_{\Gamma} \cdot \mathbf{n}_{\partial\Gamma}) \, ds. \end{aligned}$$

The corresponding function spaces are

$$\mathcal{V} = \{\mathbf{u} : \Gamma \rightarrow \mathbb{R}^3 \mid \mathbf{u} \in \mathcal{H}^1(\Gamma)^3 : \mathbf{u}_{,ji} \cdot \mathbf{n}_{\Gamma} \in \mathcal{L}^2(\Gamma)^3\} \quad (3.17)$$

$$\mathcal{V}_0 = \{\mathbf{v} \in \mathcal{V}(\Gamma) : \mathbf{v}|_{\partial\Gamma_{\text{D}}} = \mathbf{0}\} \quad (3.18)$$

where $\partial\Gamma_{\text{D}}$ is the Dirichlet boundary and $\partial\Gamma_{\text{N}}$ is the Neumann boundary. The advantage of this procedure is that the boundary terms naturally occur and directly allow to consider for mechanically meaningful boundary conditions.

3.3.2 Boundary conditions

As well known in the classical Kirchhoff-Love shell theory, special attention needs to be paid to the boundary conditions. In the following, the boundary terms of the weak form in Eq. 3.16 are rearranged in order to derive the effective boundary forces.

Using Eqs. (3.12) and (3.4), we have

$$\begin{aligned} &\int_{\partial\Gamma_{\text{N}}} \nabla_{\Gamma}^{\text{dir}}(\mathbf{v} \cdot \mathbf{n}_{\Gamma}) \cdot (\mathbf{m}_{\Gamma} \cdot \mathbf{n}_{\partial\Gamma}) - 2(\mathbf{H} \cdot \mathbf{v}) \cdot (\mathbf{m}_{\Gamma} \cdot \mathbf{n}_{\partial\Gamma}) - \mathbf{v} \cdot (\tilde{\mathbf{n}}_{\Gamma} \cdot \mathbf{n}_{\partial\Gamma}) \\ &\quad - (\mathbf{v} \cdot \mathbf{n}_{\Gamma}) (\mathbf{P} \cdot \text{div}_{\Gamma} \mathbf{m}_{\Gamma} \cdot \mathbf{n}_{\partial\Gamma}) \, ds = \\ &- \int_{\partial\Gamma_{\text{N}}} \mathbf{v} \cdot (\mathbf{n}_{\Gamma}^{\text{real}} \cdot \mathbf{n}_{\partial\Gamma}) + \mathbf{w}(\mathbf{v}) \cdot (\mathbf{m}_{\Gamma} \cdot \mathbf{n}_{\partial\Gamma}) + (\mathbf{v} \cdot \mathbf{n}_{\Gamma}) \cdot (\mathbf{P} \cdot \text{div}_{\Gamma} \mathbf{m}_{\Gamma} \cdot \mathbf{n}_{\partial\Gamma}) \, ds. \quad (3.19) \end{aligned}$$

As already mentioned above, the difference vector \mathbf{w} is a tangential vector. Consequently, the difference vector at the boundary may be expressed in terms of the tangential vectors $\mathbf{t}_{\partial\Gamma}$ and $\mathbf{n}_{\partial\Gamma}$

$$\mathbf{w}(\mathbf{v}) = \underbrace{[\nabla_{\Gamma}(\mathbf{v} \cdot \mathbf{n}_{\Gamma}) - \mathbf{H} \cdot \mathbf{v}] \cdot \mathbf{n}_{\partial\Gamma}}_{\omega_{\mathbf{t}_{\partial\Gamma}}} \mathbf{t}_{\partial\Gamma} + \underbrace{[\nabla_{\Gamma}(\mathbf{v} \cdot \mathbf{n}_{\Gamma}) - \mathbf{H} \cdot \mathbf{v}] \cdot \mathbf{t}_{\partial\Gamma}}_{\omega_{\mathbf{n}_{\partial\Gamma}}} \mathbf{n}_{\partial\Gamma} \quad (3.20)$$

where $\omega_{\mathbf{t}_{\partial\Gamma}} = \omega_{\mathbf{t}_{\partial\Gamma}} \mathbf{t}_{\partial\Gamma}$ may be interpreted as rotation along the boundary and $\omega_{\mathbf{n}_{\partial\Gamma}} = \omega_{\mathbf{n}_{\partial\Gamma}} \mathbf{n}_{\partial\Gamma}$ is the rotation in co-normal direction, when the test function \mathbf{v} is interpreted as a displacement, see Fig. 5(a). Analogously to the difference vector, the expressions $\mathbf{n}_{\Gamma}^{\text{real}} \cdot \mathbf{n}_{\partial\Gamma}$ and $\mathbf{m}_{\Gamma} \cdot \mathbf{n}_{\partial\Gamma}$ in Eq. 3.19 are decomposed in a similar manner

$$\mathbf{n}_{\Gamma}^{\text{real}} \cdot \mathbf{n}_{\partial\Gamma} = \underbrace{(\mathbf{n}_{\Gamma}^{\text{real}} \cdot \mathbf{n}_{\partial\Gamma}) \cdot \mathbf{t}_{\partial\Gamma}}_{p_{\mathbf{t}_{\partial\Gamma}}} \mathbf{t}_{\partial\Gamma} + \underbrace{(\mathbf{n}_{\Gamma}^{\text{real}} \cdot \mathbf{n}_{\partial\Gamma}) \cdot \mathbf{n}_{\partial\Gamma}}_{p_{\mathbf{n}_{\partial\Gamma}}} \mathbf{n}_{\partial\Gamma} \quad (3.21)$$

$$\mathbf{m}_{\Gamma} \cdot \mathbf{n}_{\partial\Gamma} = \underbrace{(\mathbf{m}_{\Gamma} \cdot \mathbf{n}_{\partial\Gamma}) \cdot \mathbf{n}_{\partial\Gamma}}_{m_{\mathbf{t}_{\partial\Gamma}}} \mathbf{t}_{\partial\Gamma} + \underbrace{(\mathbf{m}_{\Gamma} \cdot \mathbf{n}_{\partial\Gamma}) \cdot \mathbf{t}_{\partial\Gamma}}_{m_{\mathbf{n}_{\partial\Gamma}}} \mathbf{n}_{\partial\Gamma}. \quad (3.22)$$

Next, the term $p_{\mathbf{n}_{\Gamma}} = \mathbf{P} \cdot \text{div}_{\Gamma} \mathbf{m}_{\Gamma} \cdot \mathbf{n}_{\partial\Gamma}$ represents the resultant force in normal direction. In Fig. 5(b) the forces and bending moments along a curved boundary are illustrated.

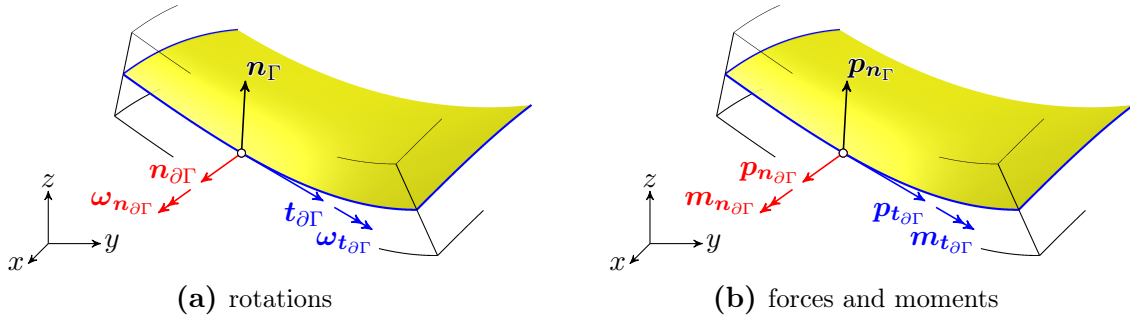


Fig. 5: Decomposition of the difference vector \mathbf{w} , in-plane normal forces $\mathbf{n}_{\Gamma}^{\text{real}} \cdot \mathbf{n}_{\partial\Gamma}$ and bending moments $\mathbf{m}_{\Gamma} \cdot \mathbf{n}_{\partial\Gamma}$ along the boundary $\partial\Gamma$ in terms of $\mathbf{t}_{\partial\Gamma}$ and $\mathbf{n}_{\partial\Gamma}$: (a) Rotations at the boundary, (b) normal force tensor and bending moments at the boundary.

Inserting these expressions in Eq. 3.19, the integral along the Neumann boundary simplifies to

$$- \int_{\partial\Gamma_N} \mathbf{v} \cdot (p_{\mathbf{t}_{\partial\Gamma}} \mathbf{t}_{\partial\Gamma} + p_{\mathbf{n}_{\partial\Gamma}} \mathbf{n}_{\partial\Gamma} + p_{\mathbf{n}_{\Gamma}} \mathbf{n}_{\Gamma}) + \omega_{\mathbf{t}_{\partial\Gamma}} m_{\mathbf{t}_{\partial\Gamma}} + \omega_{\mathbf{n}_{\partial\Gamma}} m_{\mathbf{n}_{\partial\Gamma}} \, ds. \quad (3.23)$$

As discussed in detail, e.g., in [1], the rotation in co-normal direction $\omega_{\mathbf{n}_{\partial\Gamma}}$ is already prescribed with $\mathbf{v}|_{\partial\Gamma}$. Therefore, the term $\omega_{\mathbf{n}_{\partial\Gamma}} m_{\mathbf{n}_{\partial\Gamma}}$ is expanded and with integration by parts we obtain

$$\begin{aligned} \int_{\partial\Gamma_N} \omega_{\mathbf{n}_{\partial\Gamma}} m_{\mathbf{n}_{\partial\Gamma}} \, ds &= \int_{\partial\Gamma_N} \nabla_{\Gamma}(\mathbf{v} \cdot \mathbf{n}_{\Gamma}) \cdot \mathbf{t}_{\partial\Gamma} m_{\mathbf{n}_{\partial\Gamma}} - \mathbf{H} \cdot \mathbf{v} \cdot \mathbf{t}_{\partial\Gamma} m_{\mathbf{n}_{\partial\Gamma}} \, ds \\ &= - \int_{\partial\Gamma_N} (\mathbf{v} \cdot \mathbf{n}_{\Gamma}) \cdot (\nabla_{\Gamma} m_{\mathbf{n}_{\partial\Gamma}} \cdot \mathbf{t}_{\partial\Gamma}) + \mathbf{H} \cdot \mathbf{v} \cdot \mathbf{t}_{\partial\Gamma} m_{\mathbf{n}_{\partial\Gamma}} \, ds \\ &\quad - (\mathbf{v} \cdot \mathbf{n}_{\Gamma}) m_{\mathbf{n}_{\partial\Gamma}} \Big|_{+C}^{-C} \end{aligned} \quad (3.24)$$

where $+C$ and $-C$ are points close at a corner C . The new boundary terms are the Kirchhoff forces or corner forces. Note that if the boundary of the shell is smooth, the corner forces vanish. Finally, the integral over the Neumann boundary is expressed in terms of the well-known effective boundary forces and the bending moment along the boundary

$$- \int_{\partial\Gamma_N} \mathbf{v} \cdot (\tilde{p}_{\mathbf{t}_{\partial\Gamma}} \mathbf{t}_{\partial\Gamma} + \tilde{p}_{\mathbf{n}_{\partial\Gamma}} \mathbf{n}_{\partial\Gamma} + \tilde{p}_{\mathbf{n}_{\Gamma}} \mathbf{n}_{\Gamma}) + \omega_{\mathbf{t}_{\partial\Gamma}} m_{\mathbf{t}_{\partial\Gamma}} \, ds + (\mathbf{v} \cdot \mathbf{n}_{\Gamma}) m_{\mathbf{n}_{\partial\Gamma}} \Big|_{+C}^{-C} \quad (3.25)$$

with:

$$\tilde{p}_{\mathbf{t}_{\partial\Gamma}} = p_{\mathbf{t}_{\partial\Gamma}} + (\mathbf{H} \cdot \mathbf{t}_{\partial\Gamma}) \cdot \mathbf{t}_{\partial\Gamma} m_{\mathbf{n}_{\partial\Gamma}} \quad (3.26)$$

$$\tilde{p}_{\mathbf{n}_{\partial\Gamma}} = p_{\mathbf{n}_{\partial\Gamma}} + (\mathbf{H} \cdot \mathbf{t}_{\partial\Gamma}) \cdot \mathbf{n}_{\partial\Gamma} m_{\mathbf{n}_{\partial\Gamma}} \quad (3.27)$$

$$\tilde{p}_{\mathbf{n}_{\Gamma}} = p_{\mathbf{n}_{\Gamma}} + \nabla_{\Gamma} m_{\mathbf{n}_{\partial\Gamma}} \cdot \mathbf{t}_{\partial\Gamma} . \quad (3.28)$$

The obtained effective boundary forces and moments are in agreement with the given quantities in local coordinates [1, 46]. The prescribeable boundary conditions are the conjugated displacements and rotations to the effective forces and moments at the boundary

$$\begin{aligned} \tilde{p}_{\mathbf{t}_{\partial\Gamma}} = p_{\mathbf{t}_{\partial\Gamma}} + (\mathbf{H} \cdot \mathbf{t}_{\partial\Gamma}) \cdot \mathbf{t}_{\partial\Gamma} m_{\mathbf{n}_{\partial\Gamma}} &\iff \mathbf{u} \cdot \mathbf{t}_{\partial\Gamma} = u_{\mathbf{t}_{\partial\Gamma}} , \\ \tilde{p}_{\mathbf{n}_{\partial\Gamma}} = p_{\mathbf{n}_{\partial\Gamma}} + (\mathbf{H} \cdot \mathbf{t}_{\partial\Gamma}) \cdot \mathbf{n}_{\partial\Gamma} m_{\mathbf{n}_{\partial\Gamma}} &\iff \mathbf{u} \cdot \mathbf{n}_{\partial\Gamma} = u_{\mathbf{n}_{\partial\Gamma}} , \\ \tilde{p}_{\mathbf{n}_{\Gamma}} = p_{\mathbf{n}_{\Gamma}} + \nabla_{\Gamma} m_{\mathbf{n}_{\partial\Gamma}} \cdot \mathbf{t}_{\partial\Gamma} &\iff \mathbf{u} \cdot \mathbf{n}_{\Gamma} = u_{\mathbf{n}_{\Gamma}} , \\ m_{\mathbf{t}_{\partial\Gamma}} = (\mathbf{m}_{\Gamma} \cdot \mathbf{n}_{\partial\Gamma}) \cdot \mathbf{n}_{\partial\Gamma} &\iff \omega_{\mathbf{t}_{\partial\Gamma}} = [\nabla_{\Gamma}(\mathbf{u} \cdot \mathbf{n}_{\Gamma}) - \mathbf{H} \cdot \mathbf{u}] \cdot \mathbf{n}_{\partial\Gamma} , \\ &= [(\nabla_{\Gamma}^{\text{dir}} \mathbf{u})^{\top} \cdot \mathbf{n}_{\Gamma}] \cdot \mathbf{n}_{\partial\Gamma} . \end{aligned}$$

In Tab. 1, common support types are given. Other boundary conditions (e.g., membrane

Clamped edge	$u_{\mathbf{t}_{\partial\Gamma}} = 0$	$u_{\mathbf{n}_{\partial\Gamma}} = 0$	$u_{\mathbf{n}_\Gamma} = 0$	$\omega_{\mathbf{t}_{\partial\Gamma}} = 0$
Simply supported edge	$u_{\mathbf{t}_{\partial\Gamma}} = 0$	$u_{\mathbf{n}_{\partial\Gamma}} = 0$	$u_{\mathbf{n}_\Gamma} = 0$	$m_{\mathbf{t}_{\partial\Gamma}} = 0$
Symmetry support	$\tilde{p}_{\mathbf{t}_{\partial\Gamma}} = 0$	$u_{\mathbf{n}_{\partial\Gamma}} = 0$	$\tilde{p}_{\mathbf{n}_\Gamma} = 0$	$\omega_{\mathbf{t}_{\partial\Gamma}} = 0$
Free edge	$\tilde{p}_{\mathbf{t}_{\partial\Gamma}} = 0$	$\tilde{p}_{\mathbf{n}_{\partial\Gamma}} = 0$	$\tilde{p}_{\mathbf{n}_\Gamma} = 0$	$m_{\mathbf{t}_{\partial\Gamma}} = 0$

Tab. 1: Set of common boundary conditions

support, ...) may be derived, with the quantities above, accordingly.

4 Implementational aspects

The continuous weak form is discretized using isogeometric analysis as proposed by Hughes et al. [29, 10]. The NURBS patch T is the middle surface of the shell and the elements τ_i ($i = 1, \dots, n_{\text{Elem}}$) are defined by the knot spans of the patch. The mesh is then defined by the union of the elements $\Gamma = \bigcup_{\tau \in T} \tau$.

There is a fixed set of local basis functions $\{N_i^k(\mathbf{r})\}$ of order k with $i = 1, \dots, n_k$ being the number of control points and the displacements $\{\hat{u}_i, \hat{v}_i, \hat{w}_i\}$ stored at the control points i are the degrees of freedom. Using the isoparametric concept, the shape functions $N_i^k(\mathbf{r})$ are NURBS of order k . The surface derivatives of the shape functions are computed as defined in Section 2, similar as in the surface FEM [18, 16, 20, 22] using NURBS instead of Lagrange polynomials as ansatz and test functions. The shape functions of order $k \geq 2$ are in the function space \mathcal{V} , see Eq. 3.17. In fact, the used shape functions are in the Sobolev space $\mathcal{H}^k(\Gamma)^3 \subset \mathcal{V}$ iff $k \geq 2$.

The resulting element stiffness matrix \mathbf{K}_{Elem} is a 3×3 block matrix and is divided into a membrane and bending part

$$\mathbf{K}_{\text{Elem}} = \mathbf{K}_{\text{Elem,M}} + \mathbf{K}_{\text{Elem,B}} . \quad (4.1)$$

The membrane part is defined by

$$\mathbf{K}_{\text{Elem,M}} = t \int_{\Gamma} P_{ib} \cdot [\hat{\mathbf{K}}]_{bj} \, d\Gamma \quad (4.2)$$

$$[\hat{\mathbf{K}}]_{kj} = \mu(\delta_{kj} \mathbf{N}_{,a}^\Gamma \cdot \mathbf{N}_{,a}^{\Gamma\Gamma} + \mathbf{N}_{,j}^\Gamma \cdot \mathbf{N}_{,k}^{\Gamma\Gamma}) + \lambda \mathbf{N}_{,k}^\Gamma \cdot \mathbf{N}_{,j}^{\Gamma\Gamma} , \quad (4.3)$$

summation over a and b . The matrix $\hat{\mathbf{K}}$ is determined by directional first-order derivatives

of the shape functions \mathbf{N} . One may recognize that the structure of the matrix $\hat{\mathbf{K}}$ is similar to the stiffness matrix of 3D linear elasticity problems. For the bending part we have

$$[\mathbf{K}_{\text{Elem,B}}]_{ij} = D \int_{\Gamma} n_i n_j \tilde{\mathbf{K}} \, d\Gamma \quad (4.4)$$

$$\tilde{\mathbf{K}} = (1 - \nu) \mathbf{N}_{,ab}^{\text{cov}} \cdot \mathbf{N}_{,ab}^{\text{cov}\top} + \nu \mathbf{N}_{,cc}^{\text{cov}} \cdot \mathbf{N}_{,dd}^{\text{cov}\top} . \quad (4.5)$$

A summation over a, b on the one hand and c, d on the other has to be performed. The first term of $\tilde{\mathbf{K}}$ is the contraction of the covariant Hessian matrix $\mathbf{H}\mathbf{e}_{\Gamma}^{\text{cov}}$ and the second term may be identified as the Bi-Laplace operator. Note that for the Bi-Laplace operator also directional derivatives may be used, due to the fact that the trace of second order derivatives is invariant, although the components differ. This suggests a further rearrangement of the contraction of the covariant Hessian matrix in order to use only directional derivatives, which is preferred from an implementational point of view. The equivalent expression of $\tilde{\mathbf{K}}$ using only second-order directional derivatives is

$$\tilde{\mathbf{K}} = (1 - \nu) P_{ea} \mathbf{N}_{,ab}^{\text{dir}} \cdot \mathbf{N}_{,be}^{\text{dir}\top} + \nu \mathbf{N}_{,cc}^{\text{dir}} \cdot \mathbf{N}_{,dd}^{\text{dir}\top} , \quad (4.6)$$

with summation over a, b, e and c, d as above. An example implementation for these stiffness matrices based on Matlab[®] is given in Appendix A. When the shell is given through a parametrization, the resulting element stiffness matrix in the classical theory, e.g., [9] is equivalent to the element stiffness matrix from above, but in the classical setting the computation is more cumbersome due to fact that the local basis vectors and the metric tensor in co- and contra-variant form has to be computed. In contrast, herein, the surface gradients and second-order derivatives are first applied to the shape functions (NURBS or classical finite element functions) to obtain $\mathbf{N}_{,i}^{\Gamma}$, $\mathbf{N}_{,ij}^{\text{dir}}$ and $\mathbf{N}_{,ij}^{\text{cov}}$, which is independent of the application. In this sense, a significant part of the complexity of implementing shells is shifted to finite element technology and may be recycled for any kind of boundary value problems on curved surfaces in \mathbb{R}^3 . Examples are transport problems [17, 16, 18] or flow problems [20, 30] on curved surfaces. We expect that future implementations in finite element software will provide frameworks for solving PDEs on manifolds and, based, e.g., on this work will also apply to shells.

The boundary conditions are weakly enforced by Lagrange multipliers [48]. The shape functions of the Lagrange multipliers are NURBS of the same order than the shape functions of the displacements. Therefore, the shape functions of the Lagrange multiplier i is

defined as

$$\{N_{iL}^k(\mathbf{r})\} = \{N_i^k(\mathbf{r})|_{\partial\Gamma_D}\} . \quad (4.7)$$

For the test cases shown in Section 5, bounded condition numbers and unique solutions are observed. The usual assembly yields a linear system of equations in the form

$$\begin{bmatrix} \mathbf{K} & \mathbf{C} \\ \mathbf{C}^\top & \mathbf{0} \end{bmatrix} \cdot \begin{bmatrix} \hat{\mathbf{u}} \\ \hat{\boldsymbol{\lambda}} \end{bmatrix} = \begin{bmatrix} \mathbf{f} \\ \mathbf{0} \end{bmatrix} , \quad (4.8)$$

with $[\hat{\mathbf{u}}, \hat{\boldsymbol{\lambda}}]^\top = [\hat{\mathbf{u}}, \hat{\mathbf{v}}, \hat{\mathbf{w}}, \hat{\boldsymbol{\lambda}}]$ being the sought displacements of the control points and Lagrange multipliers. With the shape functions of the Lagrange multipliers \mathbf{N}_L , the constraint matrix \mathbf{C} for simply supported edges is defined by

$$\mathbf{C}^\top = \int_{\partial\Gamma_D} \begin{bmatrix} \mathbf{N}_L \cdot \mathbf{N}^\top & \mathbf{0} & \mathbf{0} \\ \mathbf{0} & \mathbf{N}_L \cdot \mathbf{N}^\top & \mathbf{0} \\ \mathbf{0} & \mathbf{0} & \mathbf{N}_L \cdot \mathbf{N}^\top \end{bmatrix} ds , \quad (4.9)$$

for clamped edges

$$\mathbf{C}^\top = \int_{\partial\Gamma_D} \begin{bmatrix} \mathbf{N}_L \cdot \mathbf{N}^\top & \mathbf{0} & \mathbf{0} \\ \mathbf{0} & \mathbf{N}_L \cdot \mathbf{N}^\top & \mathbf{0} \\ \mathbf{0} & \mathbf{0} & \mathbf{N}_L \cdot \mathbf{N}^\top \\ \mathbf{N}_L \cdot (n_x n_{\partial\Gamma_i} \mathbf{N}_{,i}^{\Gamma\top}) & \mathbf{N}_L \cdot (n_y n_{\partial\Gamma_i} \mathbf{N}_{,i}^{\Gamma\top}) & \mathbf{N}_L \cdot (n_z n_{\partial\Gamma_i} \mathbf{N}_{,i}^{\Gamma\top}) \end{bmatrix} ds , \quad (4.10)$$

and for symmetry supports

$$\mathbf{C}^\top = \int_{\partial\Gamma_D} \begin{bmatrix} n_{\partial\Gamma_x} \mathbf{N}_L \cdot \mathbf{N}^\top & n_{\partial\Gamma_y} \mathbf{N}_L \cdot \mathbf{N}^\top & n_{\partial\Gamma_z} \mathbf{N}_L \cdot \mathbf{N}^\top \\ \mathbf{N}_L \cdot (n_x n_{\partial\Gamma_i} \mathbf{N}_{,i}^{\Gamma\top}) & \mathbf{N}_L \cdot (n_y n_{\partial\Gamma_i} \mathbf{N}_{,i}^{\Gamma\top}) & \mathbf{N}_L \cdot (n_z n_{\partial\Gamma_i} \mathbf{N}_{,i}^{\Gamma\top}) \end{bmatrix} ds . \quad (4.11)$$

Note that all constraint matrices have three block-columns referring to the unknowns $\hat{\mathbf{u}}, \hat{\mathbf{v}}, \hat{\mathbf{w}}$.

5 Numerical results

The numerical results are achieved using NURBS functions for the geometry and shape function definition, following the methodology of isogeometric analysis (IGA) [29, 31, 3,

33, 24]. The definition of NURBS is omitted here for brevity but is found at numerous references in the frame of IGA, e.g., [37, 10].

The obtained shell equations are carefully verified and compared to the classical approach with different test cases. As already mentioned above the proposed approach leads to an equivalent stiffness matrix for arbitrary curved and non-curved shells. Consequently, the same convergence properties as shown, e.g., in [31, 9] are expected. In the following, the results of the convergence analyses of a flat shell embedded in \mathbb{R}^3 , the Scordelis-Lo roof, and the pinched cylinder test (part of the shell obstacle course proposed by Belytschko et al. [2]) are shown. Furthermore, a new test case with a challenging geometry is proposed which features smooth solutions enabling higher-order convergence rates. These rates are confirmed in the residual error as no analytic solution exists, see Section 5.4. Other examples (e.g., pinched hemispherical shell, shells of revolution, etc.) have been considered but are omitted here for brevity.

In the convergence studies, NURBS patches with different orders and numbers of knot spans in each direction are employed. This is equivalent to meshes with higher-order elements and $n = \{2, 4, 8, 16, 32\}$ elements per side are used. The orders are varied as $p = \{2, 3, 4, 5, 6\}$.

5.1 Flat shell embedded in \mathbb{R}^3

Following a similar rationale as in [26], as a first test case, we consider a simple quadrilateral, flat shell with the normal vector $\mathbf{n}_\Gamma = [-1/4, -\sqrt{3}/2, \sqrt{3}/4]^\top$ in \mathbb{R}^3 , see Fig. 6. The shell is simply supported at all edges. For verification, the load vector \mathbf{f} is split into tangential \mathbf{f}_t and normal f_n loads. The tangential loads are obtained with the method of manufactured solution for a given displacement field $\mathbf{u}_t(\mathbf{x}) = [[1, 1]^\top \cdot 1/4 \cdot \sin(\pi r) \sin(\pi s)] \circ \boldsymbol{\chi}^{-1}$. In normal direction, a sinusoidal load $f_n(\mathbf{x}) = [-D \sin(\pi r) \sin(\pi s)] \circ \boldsymbol{\chi}^{-1}$ is applied to the shell. Herein, $\boldsymbol{\chi}$ is an affine mapping function (rigid-body rotation) from the horizontal parameter space to the real domain. An analytic solution for the normal displacements is easily obtained with $u_n(\mathbf{x}) = [-(\sin(\pi r) \sin(\pi s))/(4\pi^4)] \circ \boldsymbol{\chi}^{-1}$, [43]. The shell is defined with $L = 1$ and the thickness is set to $t = 0.01$. The material parameters are: Young's modulus $E = 10\,000$ and the Poisson's ratio $\nu = 0.3$.

In Fig. 7, the solution of the shell is illustrated. The displacements are scaled by two orders of magnitude. The colours on the deformed surface indicate the Euclidean norm of the

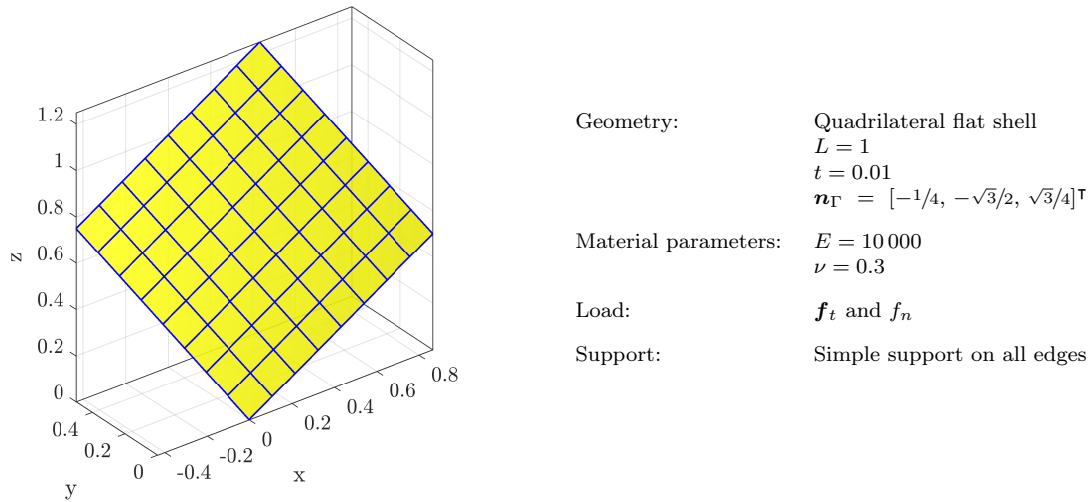


Fig. 6: Definition of flat shell problem.

displacement field $\|\mathbf{u}\|$.

The results of the convergence analysis are shown in Fig. 8. The curves are plotted as a function of the element size $1/n$ (which is rather a characteristic length of the knot spans). The dotted lines indicate the theoretical optimal order of convergence. In Fig. 8(a), the relative L_2 -error of the primal variable (displacements) is shown. Optimal higher-order convergence rates $\mathcal{O}(p+1)$ are achieved. In the figures Fig. 8(b) to Fig. 8(d), the relative L_2 -errors of the normal forces (membrane forces), bending moments and transverse shear forces are plotted. For all stress resultants the theoretical optimal orders of convergence are achieved. It is clear that the same results were obtained if the results are computed for the purely two-dimensional case as, e.g., in [9].

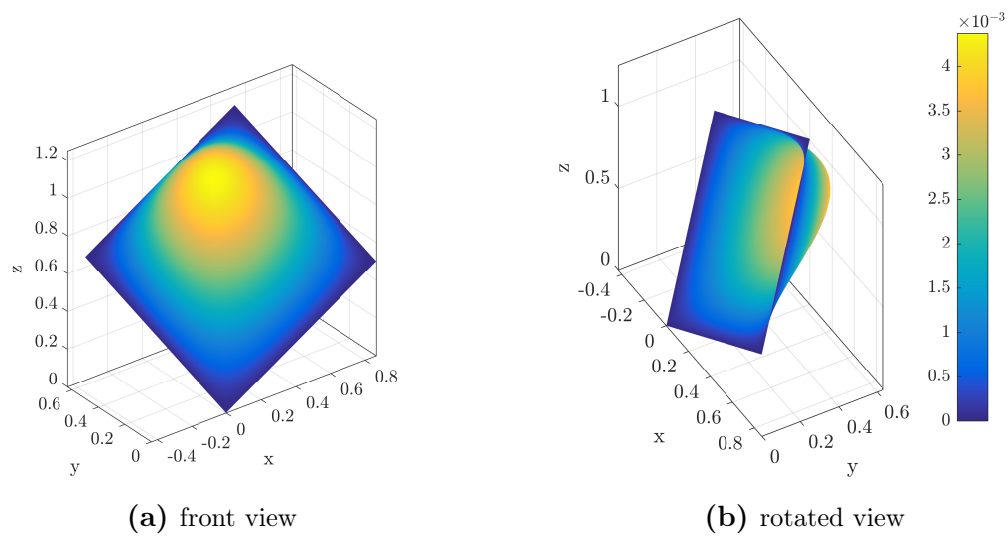
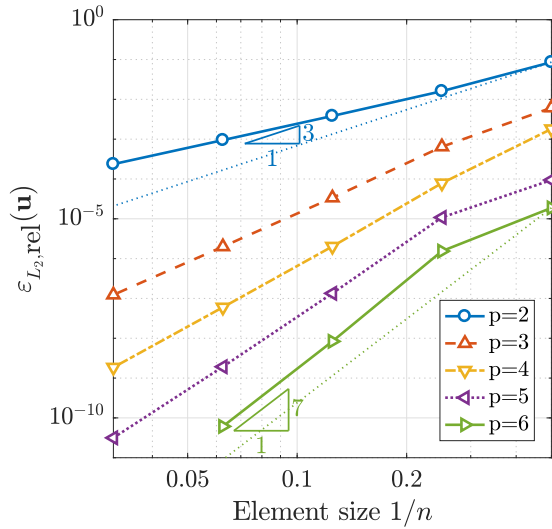
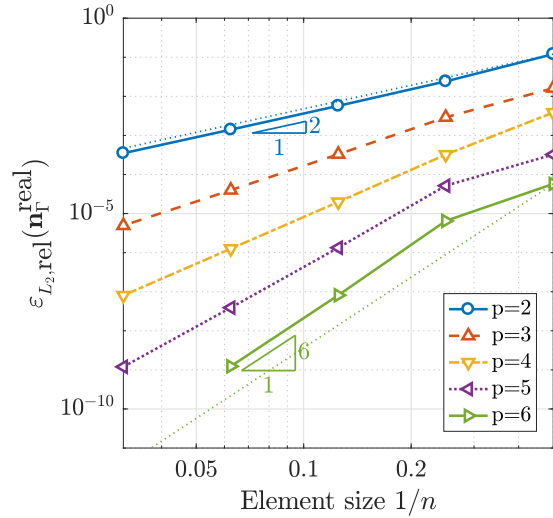


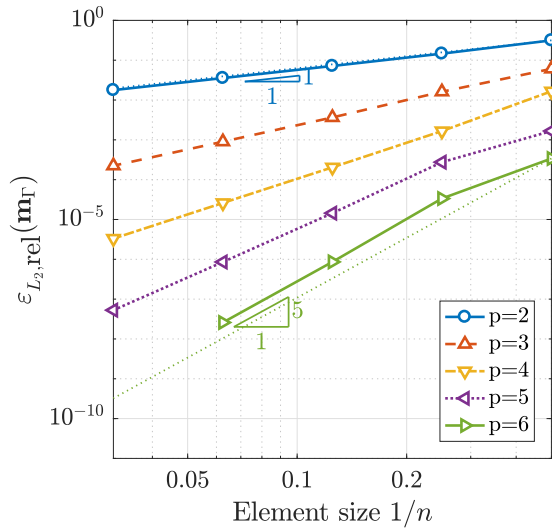
Fig. 7: Displacement u of arbitrarily orientated flat shell, scaled by two orders of magnitude.



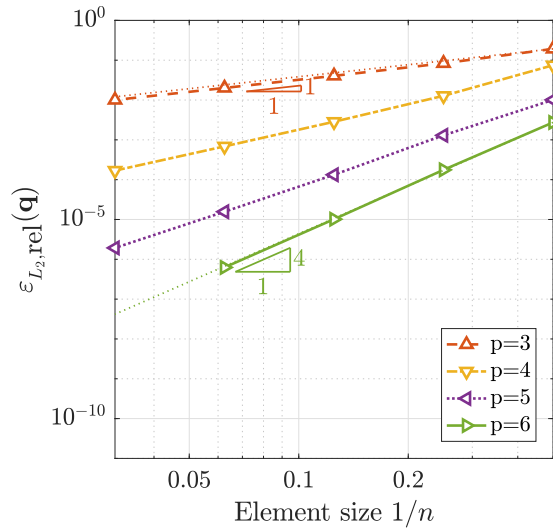
(a) Relative L_2 -norm of displacements \mathbf{u}



(b) Relative L_2 -norm of normal forces \mathbf{n}_Γ^{real}



(c) Relative L_2 -norm of bending moments \mathbf{m}_Γ

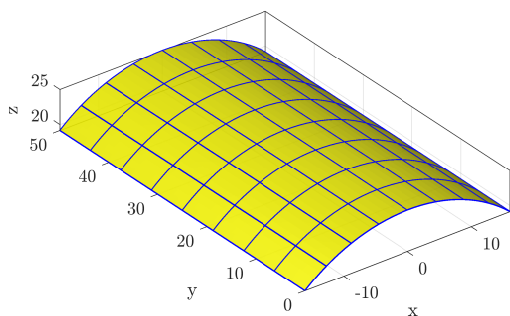


(d) Relative L_2 -norm of transverse shear forces \mathbf{q}

Fig. 8: Convergence results for the rotated flat shell.

5.2 Scordelis-Lo roof

The Scordelis-Lo roof is a cylindrical shell and is supported with two rigid diaphragms at the ends. The shell is loaded by gravity forces, see Fig. 9. The cylinder is defined with $L = 50$, $R = 25$ and the angle subtended by the roof is $\phi = 80^\circ$. The thickness of the shell is set to $t = 0.25$. The material parameters are: Young's modulus $E = 4.32 \times 10^8$ and the Poisson's ratio $\nu = 0.0$. In contrast to the first example, the maximum vertical displacement $u_{z,\max}$ is compared with the reference solution $u_{z,\max,\text{Ref}} = 0.3024$ as given in reference [2].



Geometry:	Cylindrical shell $L = 50$ $R = 25$ $\phi = 80^\circ$ $t = 0.25$
Material parameters:	$E = 4.32 \times 10^8$ $\nu = 0.0$
Load:	Gravity load $\mathbf{f} = [0, 0, -90]^\top$
Support:	Rigid diaphragms at its ends

Fig. 9: Definition of Scordelis-Lo roof problem.

In Fig. 10(a), the numerical solution of the Scordelis-Lo roof is illustrated. The displacements are magnified by one order of magnitude.

In Fig. 10(b), the convergence of the maximum displacement $u_{z,\max}$ is plotted up to polynomial order of $p = 6$ as a function of the element (knot span) size. It is clearly seen that the expected results are achieved, with increasing accuracy for higher-order NURBS. Due to the lack of a more accurate reference solutions, it is not useful to show these results in a double-logarithmic diagram as usual for error plots. The style of presentation follows those of many other references such as, e.g., in [2, 9, 31].

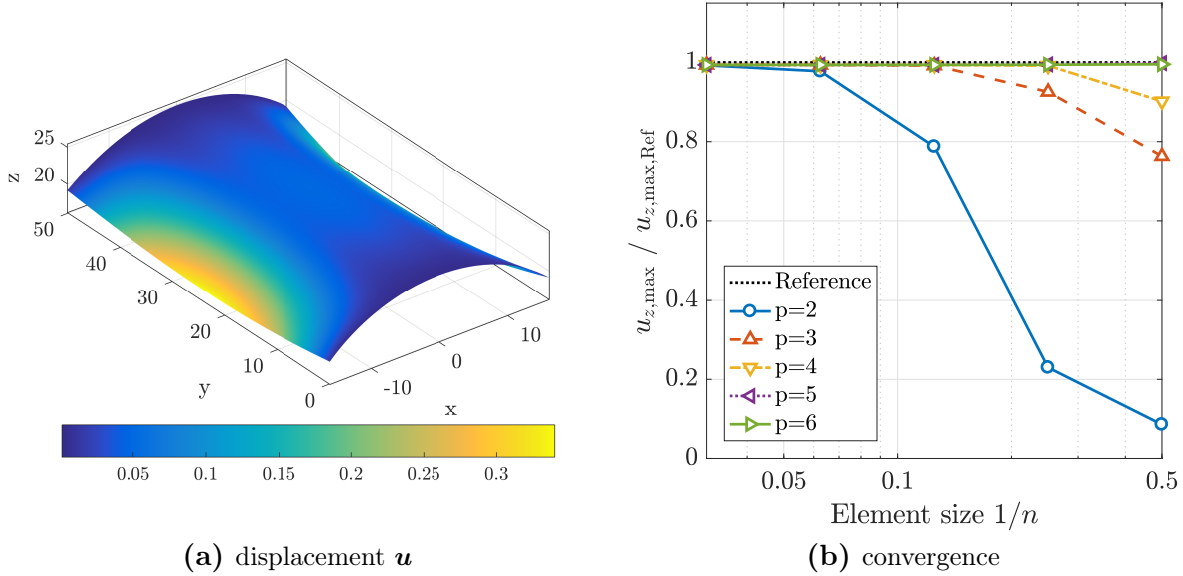


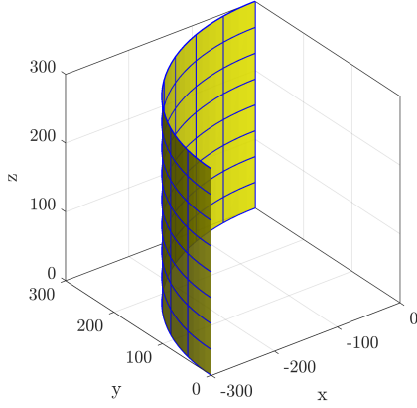
Fig. 10: (a) Displacement field of the Lo-Scordelis roof scaled by one order of magnitude, (b) normalized convergence of reference displacement $u_{z,\max,\text{Ref}} = 0.3024$.

5.3 Pinched cylinder

The next test case is a cylindrical shell pinched with two diametrically opposite unit loads located within the middle of the shell, see Fig. 11. The cylinder is defined with $L = 600$, $R = 300$. The thickness is set to $t = 3$. The material properties are: Young's modulus $E = 3 \times 10^6$ and the Poisson's ratio $\nu = 0.3$. The reference displacement at the loading points are $u_{\text{Ref}} = 1.82488 \times 10^{-5}$ as given in reference [2]. Due to symmetry only one eighth of the geometry is modelled.

In Fig. 12(a), the numerical solution of the pinched cylinder is illustrated with scaled displacements by a factor of 5×10^6 .

As in the example before, in Fig. 12(b), the convergence to a normalized reference displacement as a function of the element size is plotted. The results confirm with the expected convergence behaviour as shown in [9, 31]. It is noted that due to the singularity in some mechanical quantities due to the single force, higher-order convergence rates are not possible here. However, the improvement for increasing the order of the NURBS is still seen in the figure. An additional grading of the elements in order to better resolve the singularity would have further improved the situation but is omitted here.



Geometry:	Cylinder (one eighth of cylinder modeled) $L/2 = 300$ $R = 300$ $\phi = 90^\circ$ $t = 3$
Material parameters:	$E = 3 \times 10^6$ $\nu = 0.3$
Load:	Single unit forces
Support:	Rigid diaphragms at the top and symmetry boundary conditions

Fig. 11: Definition of the pinched cylinder problem.

5.4 Flower shaped shell

As a last example, a more complex geometry is considered, which enables smooth mechanical fields and thereby enables higher-order convergence rates. The geometry of the middle surface is given with

$$\mathbf{x}_\Gamma(r, s) = \begin{bmatrix} (A - C) \cos(\theta) \\ (A - C) \sin(\theta) \\ 1 - s^2 \end{bmatrix} \quad \text{with: } r, s \in [-1, 1], A = 2.3, B = 0.8 \quad (5.1)$$

$$\theta(r) = \pi(r + 1)$$

$$C(r, s) = s[B + 0.3 \cos(6\theta)]$$

and illustrated in Fig. 13. On the right side of the figure, the boundary conditions and material parameters are defined. The middle surface of the shell features varying principle curvatures and curved boundaries. The curved boundaries are clamped and the corresponding conditions (from Tab. 1) have to be properly enforced. An analytical solution or reference displacement is not available. Therefore, the error is measured in the strong form of the equilibrium from Eq. 3.13 and may be called residual error. In particular, the residual error is the summed element-wise relative L_2 -error

$$\varepsilon_{\text{rel,residual}} = \sum_{i=1}^{n_{\text{Elem}}} \varepsilon_{L_2,\text{rel},\tau_i} \quad (5.2)$$

$$\varepsilon_{L_2,\text{rel},\tau}^2 = \frac{\int_\Gamma \left\{ \text{div}_\Gamma \tilde{\mathbf{n}}_\Gamma + \mathbf{n}_\Gamma \text{div}_\Gamma (\mathbf{P} \cdot \text{div}_\Gamma \mathbf{m}_\Gamma) + 2\mathbf{H} \cdot \text{div}_\Gamma \mathbf{m}_\Gamma + [\partial x_i^\Gamma \mathbf{H}]_{jk} [\mathbf{m}_\Gamma]_{ki} + \mathbf{f} \right\}^2 d\Gamma}{\int_\Gamma \mathbf{f}^2 d\Gamma}.$$

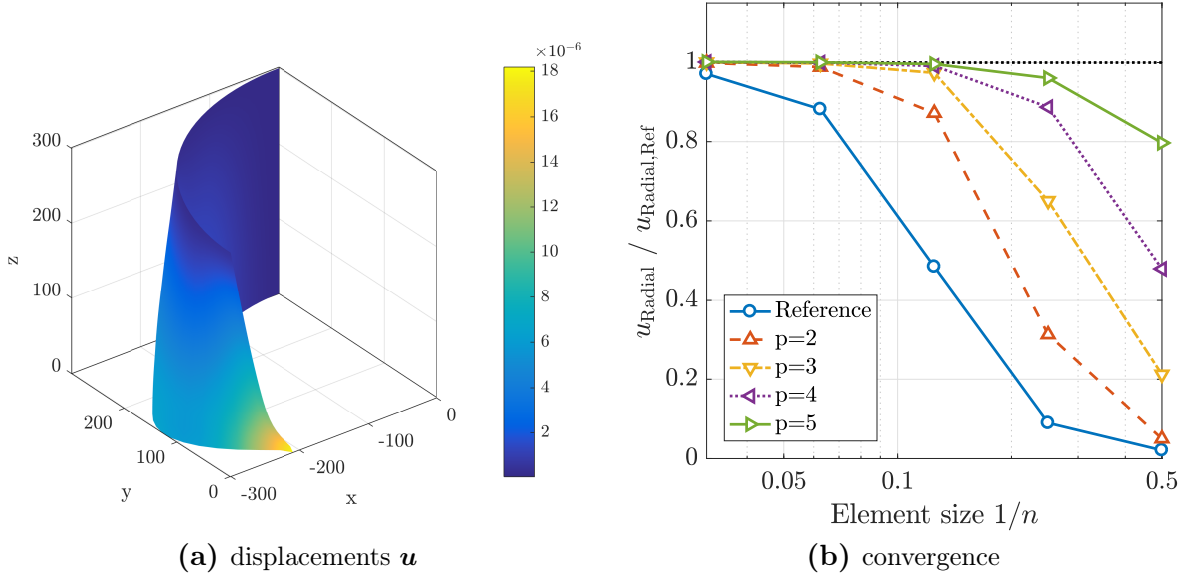


Fig. 12: Pinched cylinder: (a) Displacement \mathbf{u} of one eighth of the geometry (scaled by a factor of 5×10^6), (b) Normalized convergence of reference displacement $u_{\text{Radial,Ref}} = 1.82488 \times 10^{-5}$ at loading points.

The computation of the residual error requires the evaluation of fourth-order surface derivatives. It is noteworthy that the implementation of these higher-order derivatives is not without efforts. For example, recall that mixed directional surface derivatives are not symmetric. That is, there are $3^4 = 81$ partial fourth-order derivatives. Nevertheless, if the displacement field is smooth enough this error measure is a suitable quantity for the convergence analysis.

In Fig. 14(a), the deformed shell is illustrated. The displacement field is scaled by one order of magnitude. In Fig. 14(b), the results of the convergence analysis are plotted. Due to the fact that fourth-order derivatives need to be computed, at least fourth-order shape functions are required. The theoretical optimal order of convergence is $\mathcal{O}(p - 3)$ if the solution is smooth enough. One may observe that higher-order convergence rates are achieved, however, rounding-off errors and the conditioning may slightly influence the convergence. Nevertheless, the results are excellent also given the fact that higher-order accurate results for shells (given in double-logarithmic error plots) are the exception.

The stored elastic energy at the finest level with a polynomial order $p = 8$, which may be seen as an overkill solution, is $\epsilon = 1.917780305921 \pm 1 \times 10^{-13}$ kN m. This stored elastic energy may be used for future benchmark tests, without the need to implement fourth-order

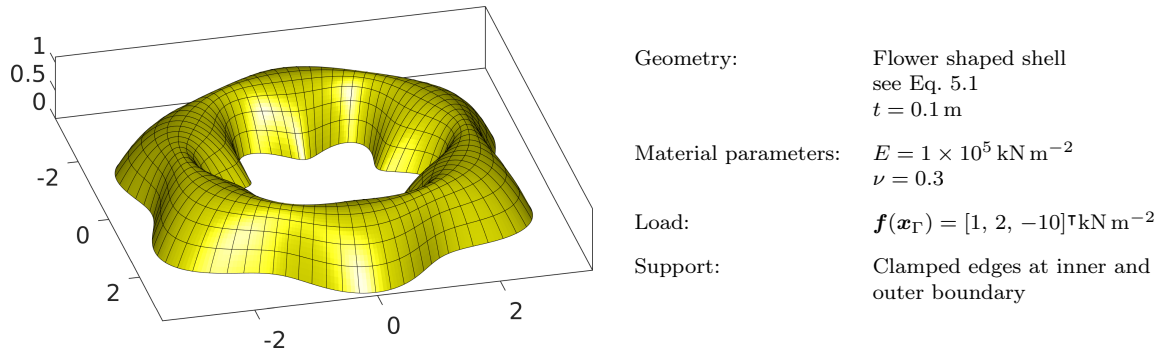


Fig. 13: Definition of flower shaped shell problem

derivatives on manifolds.

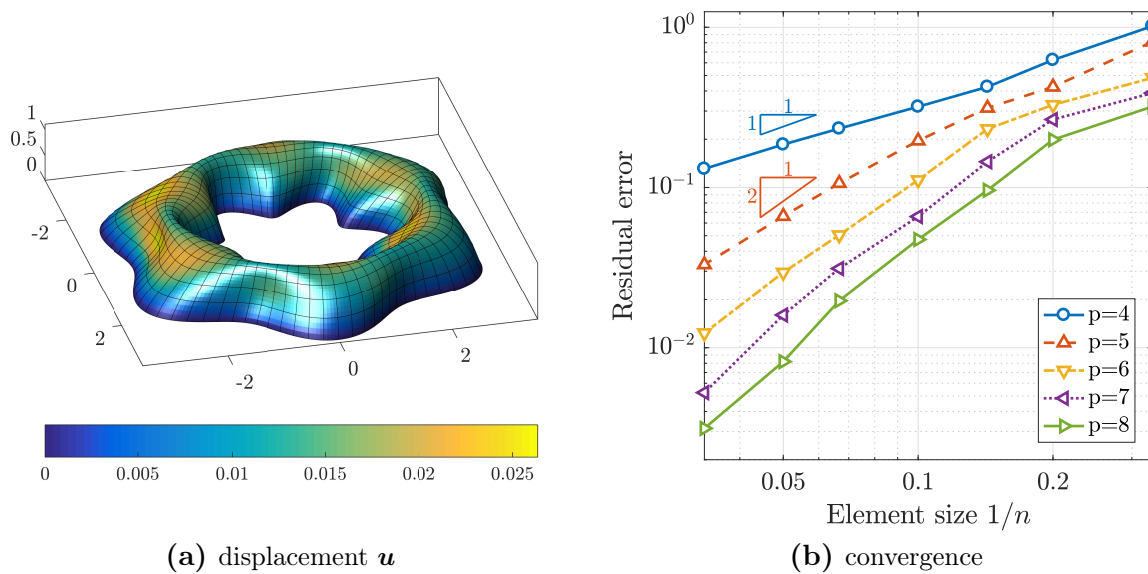


Fig. 14: Flower shaped shell: (a) Displacement \mathbf{u} of flower shaped shell (scaled by one order of magnitude), (b) Residual error $\varepsilon_{\text{rel, residual}}$.

6 Conclusions and Outlook

We have presented a reformulation of the linear Kirchhoff-Love shell theory in terms of the TDC using a global Cartesian coordinate system and tensor notation. The obtained equations do not hinge on a parametrization of the middle surface of the shell, which may be seen as a generalization of the classical shell equations. The parameter-free strong form is

used as the starting point to consistently obtain the weak form including all boundary terms well-known in the Kirchhoff-Love theory. Mechanical stress-resultants such as moments, normal and shear forces are defined in global coordinates. Furthermore, the strong form may be used in the numerical results to compute residual errors and thus enable convergence analyses even without the knowledge of exact solutions which, for shells, are scarce.

For the discretization, the surface FEM is used with NURBS as trial and test functions. In comparison to the classical theory, the reformulation leads to a more compact and intuitive implementation and *only* directional derivatives need to be computed explicitly. The numerical results confirm that the proposed formulation is equivalent to the classical formulation and higher-order convergence rates are achieved. As mentioned, based on the residual errors, a framework for the verification of complex test cases is presented.

There is a large potential in the parameter-free reformulation of the shell models, because the obtained PDEs may be discretized with new finite element techniques such as Trace-FEM or CutFEM based on implicitly defined surfaces. In this case, neither the problem-statement nor the discretization is based on a parametrization. For the weak enforcement of the boundary conditions, Nitsche's method or penalty methods shall be used.

A Element stiffness matrix

In order to clarify the implementation, we give the Matlab-code of the routine which evaluates the element contribution to the matrix and right hand side. The input contains the shape function data and normal vectors evaluated at the integration points plus the material parameters. Note that the first- and second-order surface derivatives are included in the shape function data, i.e., $\nabla_{\Gamma} N_i(\mathbf{x}_j)$ and $\mathbf{H}\mathbf{e}^{\text{cov}}(N_i(\mathbf{x}_j))$ where $i = 1, \dots, n$ refers to the n shape functions in the current element (knot span) and \mathbf{x}_j with $j = 1, \dots, m$ to integration points. The computation of these quantities is part of the standard finite element technology provided by the implementation and is independent of the application to shells.

```

function [ElemMat, ElemRhs] = GetElementContributionShell(...
ShapeFcts, ipReal, Parameters, NormalVectors)

% Compute element stiffness matrix.
%
% Input variables:
% ShapeFcts is a data structure storing shape functions and their surface
% derivatives as members. Each member is an (n x m)-matrix of n shape
% functions evaluated at m integration points. Existing members:
% -ShapeFcts.NodeNum: Number n of shape functions in this element/know span.
% -ShapeFcts.f: shape functions (e.g., NURBS or classical FE functions).
% -ShapeFcts.fx, .fy, .fz: Surface gradient applied to each shape function.
% -ShapeFcts.fxx, .fyy, .fzz, .fxy, .fzx, .fyz: *Covariant* 2nd derivatives
% of the shape functions.
% ipReal stores the integration points and weights in members:
% -ipReal.nQ: Number of integration points.
% -ipReal.xx, ipReal.yy, ipReal.zz: Coordinates of integration points.
% -ipReal.w: Integration weights.
% Parameters stores material parameters.
% NormalVectors is a matrix with 3 columns storing the normal vector
% components at each integration point.
%
% Output variables:
% ElemMat: Element matrix of size (n x n).
% ElemRhs: Element right hand side of size (n x 1).

nn = ShapeFcts.NodeNum;
ElemMat = zeros(3*nn, 3*nn); % Size of element matrix.
ElemRhs = zeros(3*nn, 1); % Size of element right hand side.

% Material parameters.
DD = Parameters.DD;
nu = Parameters.nu;
mu = Parameters.mu;
lambda = Parameters.lambda;
tt = Parameters.tt;

% Loading in x-, y-, z-direction evaluated at integration points.
[fx, fy, fz] = EvaluateLoad(ipReal.xx, ipReal.yy, ipReal.zz);

% Loop over integration points.
for i = 1 : ipReal.nQ

% Read out shape functions and derivatives at current integration point.
N = ShapeFcts.f(:, i);
Nx = ShapeFcts.fx(:, i); Ny = ShapeFcts.fy(:, i); Nz = ShapeFcts.fz(:, i);
Nxx = ShapeFcts.fxx(:, i); Nyy = ShapeFcts.fyy(:, i); Nzz = ShapeFcts.fzz(:, i);
Nxy = ShapeFcts.fxy(:, i); Nxz = ShapeFcts.fxz(:, i); Nyz = ShapeFcts.fyz(:, i);

% Define projectors, (3x3)-matrices:
Q = NormalVectors(i, :) * NormalVectors(i, :);
P = eye(3,3) - Q;

% Membrane stiffness, contribution at integration point.
Mat11 = (lambda+2*mu) * Nx*Nx' + mu * Ny*Ny' + mu * Nz*Nz';
Mat12 = lambda * Nx*Ny' + mu * Ny*Nx';
Mat13 = lambda * Nx*Nz' + mu * Nz*Nx';

Mat21 = lambda * Ny*Nx' + mu * Nx*Ny';
Mat22 = (lambda+2*mu) * Ny*Ny' + mu * Nx*Nx' + mu * Nz*Nz';
Mat23 = lambda * Ny*Nz' + mu * Nz*Ny';

Mat31 = lambda * Nz*Nx' + mu * Nx*Nz';
Mat32 = lambda * Nz*Ny' + mu * Ny*Nz';
Mat33 = (lambda+2*mu) * Nz*Nz' + mu * Nx*Nx' + mu * Ny*Ny';

KKmemb11 = P(1,1)*Mat11 + P(1,2)*Mat21 + P(1,3)*Mat31;
KKmemb12 = P(1,1)*Mat12 + P(1,2)*Mat22 + P(1,3)*Mat32;
KKmemb13 = P(1,1)*Mat13 + P(1,2)*Mat23 + P(1,3)*Mat33;

KKmemb21 = P(2,1)*Mat11 + P(2,2)*Mat21 + P(2,3)*Mat31;
KKmemb22 = P(2,1)*Mat12 + P(2,2)*Mat22 + P(2,3)*Mat32;
KKmemb23 = P(2,1)*Mat13 + P(2,2)*Mat23 + P(2,3)*Mat33;

```

```

KKmemb31 = P(3,1)*Mat11 + P(3,2)*Mat21 + P(3,3)*Mat31;
KKmemb32 = P(3,1)*Mat12 + P(3,2)*Mat22 + P(3,3)*Mat32;
KKmemb33 = P(3,1)*Mat13 + P(3,2)*Mat23 + P(3,3)*Mat33;

KKmemb = tt * [...
KKmemb11 KKmemb12 KKmemb13;
KKmemb21 KKmemb22 KKmemb23;
KKmemb31 KKmemb32 KKmemb33;
];

% Bending stiffness, contribution at integration point.
% ...covariant Hesse contraction (with covariant derivatives)
K1 = Nxx*Nxx' + Nyy*Nyy' + Nzz*Nzz' + 2*(Nxy*Nxy' + Nxz*Nxz' + Nyz*Nyz');
% ...Bi-Laplace-Beltrami
K2 = (Nxx+Nyy+Nzz) * (Nxx+Nyy+Nzz)';
MatWW = (1-nu) * K1 + nu * K2;

KKbend = DD * [...
MatWW*Q(1,1) MatWW*Q(1,2) MatWW*Q(1,3); ...
MatWW*Q(2,1) MatWW*Q(2,2) MatWW*Q(2,3); ...
MatWW*Q(3,1) MatWW*Q(3,2) MatWW*Q(3,3)];

% Right hand side, contribution at integration point.
Rhs1 = N * fx(i);
Rhs2 = N * fy(i);
Rhs3 = N * fz(i);
Rhs = [Rhs1; Rhs2; Rhs3];

% Add contribution at integration point to element matrix and rhs.
ElemMat = ElemMat + ipReal.ww(i) * (KKmemb + Kkbend);
ElemRhs = ElemRhs + ipReal.ww(i) * Rhs;

end

function [fx, fy, fz] = EvaluateLoad(xx, yy, zz)

nn = length(xx);
fx = zeros(nn, 1);
fy = zeros(nn, 1);
fz = zeros(nn, 1);

end

```

References

- [1] Bařar, Y.; Krätzig, W.B.: *Mechanik der Flächentragwerke*. Vieweg+Teubner Verlag, Braunschweig, 1985.
- [2] Belytschko, T.; Stolarski, H.; Liu, W.K.; Carpenter, N.; Ong, J.S.J: Stress projection for membrane and shear locking in shell finite elements. *Comp. Methods Appl. Mech. Engrg.*, **51**, 221–258, 1985.
- [3] Benson, D.J.; Bazilevs, Y.; Hsu, M.C.; Hughes, T.J.R.: Isogeometric shell analysis: The Reissner-Mindlin shell. *Comp. Methods Appl. Mech. Engrg.*, **199**, 276–289, 2010.
- [4] Bischoff, M.; Bletzinger, K.U.; Wall, W.A.; Ramm, E.: Models and Finite Elements for Thin-Walled Structures. *Encyclopedia of Computational Mechanics*, John Wiley & Sons, Chichester, Chapter 3, 2004.
- [5] Blaauwendraad, J.; Hoefakker, J.H.: *Structural Shell Analysis*, Vol. 200, *Solid Mechanics and Its Applications*. Springer, Berlin, 2014.
- [6] Burman, E.; Claus, S.; Hansbo, P.; Larson, M.G.; Massing, A.: CutFEM: Discretizing geometry and partial differential equations. *Internat. J. Numer. Methods Engrg.*, **104**, 472–501, 2015.
- [7] Burman, E.; Elfverson, D.; Hansbo, P.; Larson, M.G.; Larsson, K.: Shape optimization using the cut finite element method. *Comp. Methods Appl. Mech. Engrg.*, **328**, 242–261, 2018.
- [8] Cenanovic, M.; Hansbo, P.; Larson, M.G.: Cut finite element modeling of linear membranes. *Comp. Methods Appl. Mech. Engrg.*, **310**, 98–111, 2016.
- [9] Cirak, F.; Ortiz, M.; Schröder, P.: Subdivision surfaces: A new paradigm for thin-shell finite-element analysis. *Internat. J. Numer. Methods Engrg.*, **47**(12), 2039–2072, 2000.
- [10] Cottrell, J.A.; Hughes, T.J.R.; Bazilevs, Y.: *Isogeometric Analysis: Toward Integration of CAD and FEA*. John Wiley & Sons, Chichester, 2009.
- [11] Delfour, M.C.; Zolésio, J.P.: Shape Analysis via Oriented Distance Functions. *J. Funct. Anal.*, **123**, 129–201, 1994.

-
- [12] Delfour, M.C.; Zolésio, J.P.: A Boundary Differential Equation for Thin Shells. *J. Differential Equations*, **119**, 426–449, 1995.
- [13] Delfour, M.C.; Zolésio, J.P.: Tangential Differential Equations for Dynamical Thin Shallow Shells. *J. Differential Equations*, **128**, 125–167, 1996.
- [14] Delfour, M.C.; Zolésio, J.P.: Differential equations for linear shells comparison between intrinsic and classical. *Advances in Mathematical Sciences: CRM's 25 Years (Montreal, PQ, 1994)*, CRM Proc. Lecture Notes, Vol. 11, Providence, Rhode Island, 1997.
- [15] Delfour, M.C.; Zolésio, J.P.: *Shapes and Geometries: Metrics, Analysis, Differential Calculus, and Optimization*. SIAM, Philadelphia, PA, 2011.
- [16] Demlow, A.: Higher-order finite element methods and pointwise error estimates for elliptic problems on surfaces. *SIAM J. Numer. Anal.*, **47**, 805–827, 2009.
- [17] Dziuk, G.: *Finite Elements for the Beltrami operator on arbitrary surfaces*, Chapter 6, 142–155. Springer Berlin Heidelberg, Berlin, Heidelberg, 1988.
- [18] Dziuk, G.; Elliott, C.M.: Finite element methods for surface PDEs. *Acta Numerica*, **22**, 289–396, 2013.
- [19] Elfverson, D.; Larson, M.G.; Larsson, K.: A New Least Squares Stabilized Nitsche Method for Cut Isogeometric Analysis. *ArXiv e-prints*, 2018. ArXiv: 1804.05654.
- [20] Fries, T.P.: Higher-order surface FEM for incompressible Navier-Stokes flows on manifolds. *Int. J. Numer. Methods Fluids*, 1–24, 2018. Article in Press.
- [21] Fries, T.P.; Omerović, S.; Schöllhammer, D.; Steidl, J.: Higher-order meshing of implicit geometries - Part I: Integration and interpolation in cut elements. *Comp. Methods Appl. Mech. Engrg.*, **313**, 759–784, 2017.
- [22] Fries, T.P.; Schöllhammer, D.: Higher-order meshing of implicit geometries - part II: Approximations on manifolds. *Comp. Methods Appl. Mech. Engrg.*, **326**, 270–297, 2017.
- [23] Grande, J.; Reusken, A.: A higher order finite element method for partial differential equations on surfaces. *SIAM*, **54**, 388–414, 2016.

-
- [24] Guo, Y.; Ruess, M.; Schillinger, D.: A parameter-free variational coupling approach for trimmed isogeometric thin shells. *Comput. Mech.*, **59**, 693–715, 2017.
- [25] Hansbo, P.; Larson, M.G.: Finite element modeling of a linear membrane shell problem using tangential differential calculus. *Comp. Methods Appl. Mech. Engrg.*, **270**, 1–14, 2014.
- [26] Hansbo, P.; Larson, M.G.: Continuous/discontinuous finite element modelling of Kirchhoff plate structures in \mathbb{R}^3 using tangential differential calculus. *Comput. Mech.*, **60**, 693–702, 2017.
- [27] Hansbo, P.; Larson, M.G.; Larsson, F.: Tangential differential calculus and the finite element modeling of a large deformation elastic membrane problem. *Comput. Mech.*, **56**, 87–95, 2015.
- [28] Hansbo, P.; Larson, M.G.; Larsson, K.: Variational formulation of curved beams in global coordinates. *Comput. Mech.*, **53**, 611–623, 2014.
- [29] Hughes, T.J.R.; Cottrell, J.A.; Bazilevs, Y.: Isogeometric analysis: CAD, finite elements, NURBS, exact geometry and mesh refinement. *Comp. Methods Appl. Mech. Engrg.*, **194**, 4135–4195, 2005.
- [30] Jankuhn, T.; Olshanskii, M.A.; Reusken, A.: Incompressible Fluid Problems on Embedded Surfaces Modeling and Variational and Formulations. *ArXiv e-prints*, 2017. ArXiv: 1702.02989.
- [31] Kiendl, J.; Bletzinger, K.-U.; Linhard, J.; Wüchner, R.: Isogeometric shell analysis with Kirchhoff–Love elements. *Comp. Methods Appl. Mech. Engrg.*, **198**, 3902–3914, 2009.
- [32] Lebedzik, C.: Exact boundary controllability of a shallow intrinsic shell model. *J. Math. Anal. Appl.*, **335**, 584–614, 2007.
- [33] Nguyen, V.P.; Anitescu, C.; Bordas, S.P.A.; Rabczuk, T.: Isogeometric analysis: An overview and computer implementation aspects. *Math. Comput. Simulation*, **117**, 89–116, 2015.
- [34] Olshanskii, M.A.; Reusken, A.: Trace finite element methods for PDEs on surfaces. *Lecture Notes in Computational Science and Engineering*, **121**, 211–258, 2017.

-
- [35] Olshanskii, M.A.; Xu, X.: A trace finite element method for PDEs on evolving surfaces. *SIAM*, **39**, A1301–A1319, 2017.
- [36] Osher, S.; Fedkiw, R.P.: *Level Set Methods and Dynamic Implicit Surfaces*. Springer, Berlin, 2003.
- [37] Piegl, L.; Tiller, W.: *The NURBS Book (Monographs in Visual Communication)*. Springer, Berlin, 2 edition, 1997.
- [38] Radwańska, M.; Stankiewicz, A.; Wosatko, A.; Pamin, J.: *Plate and Shell Structures*. John Wiley & Sons, Chichester, 2017.
- [39] Reusken, A.: Analysis of trace finite element methods for surface partial differential equations. *IMA J. Numer. Anal.*, **35**, 1568–1590, 2014.
- [40] Sethian, J.A.: *Level Set Methods and Fast Marching Methods*. Cambridge University Press, Cambridge, 2 edition, 1999.
- [41] Simo, J.C.; Fox, D.D.: On a stress resultant geometrically exact shell model. Part I: Formulation and optimal parametrization. *Comp. Methods Appl. Mech. Engrg.*, **72**, 267–304, 1989.
- [42] Simo, J.C.; Fox, D.D.; Rifai, M.S.: On a stress resultant geometrically exact shell model. Part II: The linear theory; Computational aspects. *Comp. Methods Appl. Mech. Engrg.*, **73**, 53–92, 1989.
- [43] Timoshenko, S.; Woinowsky-Krieger, S.: *Theory of Plates and Shells*. McGraw-Hill Book Company, Inc., New York, 2 edition, 1959.
- [44] van Opstal, T.M.; van Brummelen, E.H.; van Zwieten, G.J.: A finite-element/boundary-element method for three-dimensional, large-displacement fluid–structure-interaction. *Comp. Methods Appl. Mech. Engrg.*, **284**, 637–663, 2015.
- [45] Walker, S.W.: *The Shapes of Things: A Practical Guide to Differential Geometry and the Shape Derivative*. Advances in Design and Control. SIAM, 2015.
- [46] Wempner, G.; Talaslidis, D.: *Mechanics of Solids and Shells: Theories and Approximations*. CRC Press LLC, Boca Raton, Florida, 2002.

-
- [47] Yao, P.F.: On shallow shell equations. *Discrete Contin. Dyn. Syst. Ser. S*, **2**, 697–722, 2009.
- [48] Zienkiewicz, O.; Taylor, R.; Zhu, J.Z.: *The Finite Element Method: Its Basis and Fundamentals: Seventh Edition*. Elsevier LTD, Oxford, 7 edition, 2013.